Two-Layer Rotating Exchange Flow between Two Deep Basins: Theory and Application to the Strait of Gibraltar

M.-L. E. TIMMERMANS AND L. J. PRATT

Woods Hole Oceanographic Institution, Woods Hole, Massachusetts

(Manuscript received 14 November 2004, in final form 1 March 2005)

ABSTRACT

Rotating two-layer exchange flow over a sill in a strait separating two relatively deep and wide basins is analyzed. Upstream of the sill in the deep upstream basin, the infinitely deep dense lower layer is assumed to be inactive, while the relatively thin upper layer flowing away from the sill forms a detached boundary current in the upstream basin. This analysis emphasizes the importance of this upstream boundary current, incorporating its width as a key parameter in a formalism for deducing the volume exchange rate and discriminating between maximal and submaximal states. Hence, even for narrow straits in which rotation does not dominate the dynamics within the strait, the importance of rotation in the wide upstream basin can be exploited. It is shown that the maximal allowable exchange transport through straits wider than 1½ Rossby deformation radii increases as rotation increases, unlike for smaller rotations, where the exchange decreases as rotation increases. The theory is applied to the exchange flow through the Strait of Gibraltar. This application illustrates how images of the oceans taken from space showing the width of the upstream flow, in this case a space shuttle photograph, might be used to determine the exchange transport through a strait. Maximal exchange conditions in the Strait of Gibraltar are predicted to apply at the time the space shuttle photograph was taken.

1. Introduction

Rotating hydraulic models are traditionally based on 1½-layer stratification and are aimed at applications involving deep overflows such as those of the Denmark Strait and Faroe Bank Channel. The overlying fluid is assumed to be relatively thick and dynamically inactive. In reality, the thicknesses of the overflows across the sills of the Denmark Strait and Faroe Bank Channel are comparable with those of the overlying fluid and Froude numbers based on the upper-layer properties are not always small (D. Sutherland and J. Girton 2004, personal communication). The importance of the upper layer is acknowledged in other applications such as the exchange flows of the Strait of Gibraltar (e.g., Armi and Farmer 1988) and the Bab al Mandab (e.g., Smeed 2000; Pratt et al. 2000). These straits have widths on the order of or less than the Rossby radius of deformation and the effects of rotation are generally neglected. However, rotation becomes dominant as the strait widens into the neighboring open ocean or marginal sea.

The situation described above suggests the need for two-layer hydraulic models that account for the effects of rotation. Some work along these lines has already been carried out. Whitehead et al. (1974) and Hunkins and Whitehead (1992) analyzed the flow that sets up in a hypothetical lock exchange experiment in a channel with a horizontal bottom. Hogg (1983) used a 2½-layer model to partition the Vema Channel overflow into two active layers and examined changes in isopycnals caused by flow over the deep sill. Hogg (1985) applied a similar model to the Alboran Sea and Strait of Gibraltar system. He considered three layers, with the lowest Deep Mediterranean Water at rest and applied the concepts of a second-mode control section in a narrow passage in the Alboran Sea to understand circulation patterns in the western Mediterranean Sea. Both studies were site-specific investigations of particular observed phenomena and the models used were quite complicated. A more general investigation of two-layer, rotating channel flow appears in the Ph.D. thesis of Dalziel (1988) and in Dalziel (1990). Attention is focused primarily on configurations that maximize the exchange

Corresponding author address: M.-L. Timmermans, MS#21, WHOI, Woods Hole, MA 02453.
E-mail: mtimmermans@whoi.edu

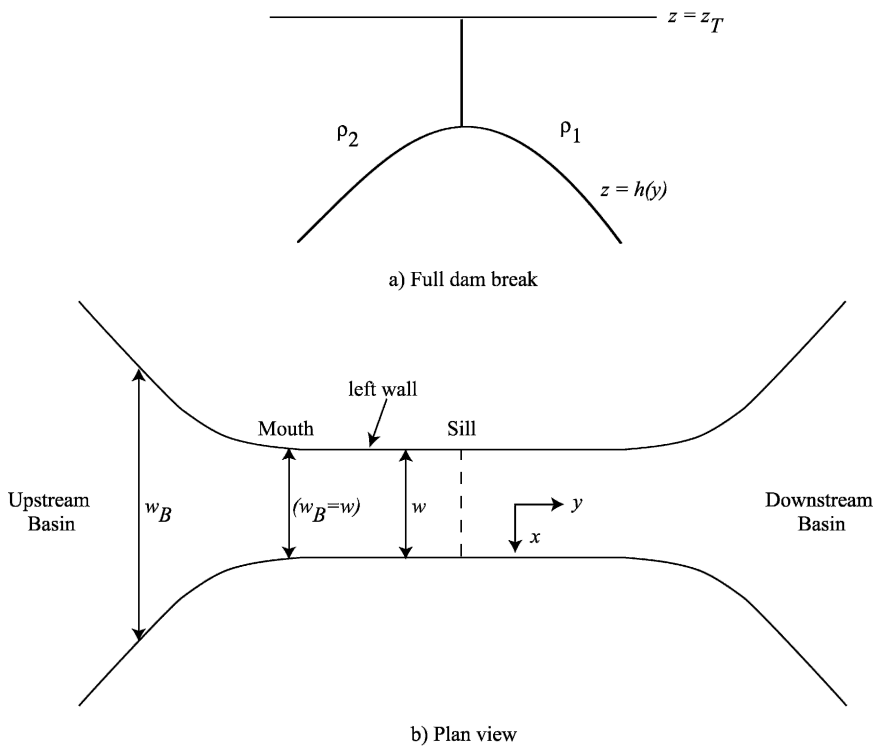

FIG. 1. Schematic showing a dam restraining fluid in the region $y < 0$. We investigate the final steady state after the dam break and the spilling of dense ρ_2 fluid over the sill. A rigid lid is placed at $z = z_T$ so there can be no free-surface gravity waves. These waves would propagate much faster than typical exchange flows so the associated Froude number would be negligible. The channel has uniform width w and is aligned in the y direction.

flow rate through a channel with a sill, the so-called maximal states. Riemenschneider (2004) has also investigated two-layer, rotating exchange flows and has carried out a series of primitive equation experiments for exchange across a sill in a strait separating two wide basins. Riemenschneider (2004) and Riemenschneider et al. (2005, manuscript submitted to *J. Fluid Mech.*) trace maximal and submaximal flows along a rectangular channel in a graphical representation analogous to the Froude number plane used by Armi (1986) and Armi and Farmer (1986).

Our investigation centers on rotating, two-layer exchange flow over a sill in a strait separating two relatively deep and wide basins. The basin serving as the source of the lower layer will be called the upstream basin and "left" and "right" will refer to the channel walls as seen by an observer facing in the direction of the lower-layer transport (Fig. 1). Here, we cover the theory for pure exchange flow and conclude with an application to the Strait of Gibraltar. Our work differs from that of Dalziel (1988, 1990), Riemenschneider (2004) and Riemenschneider et al. (2005, manuscript submitted to *J. Fluid Mech.*) in several important respects. The first is our emphasis on submaximal states, which are thought to be important in applications such as the Faroe Bank Channel and the Bab al Mandab. A more important difference involves our view of and emphasis on the upstream flow. As one moves upstream from our sill through the strait and into the deep upstream basin, the lower layer is assumed to become infinitely deep and inactive. The upper layer, which is relatively thin, remains in motion and detaches from the right wall, forming a detached boundary current on the left wall of the basin. The width of this current can be used as the basis for a weir relation determining the volume exchange rate. The width could be determined using an image from space where it could be observed as a sea-surface expression and this might therefore allow remote monitoring of the exchange transport.

Inherent in this description are assumptions concerning the potential vorticity of the flow that are quite different from what Dalziel, Riemenschneider, and coworkers have used. In their analysis, the potential vorticity of both layers is formally taken to be zero. A consequence is that the relative vorticity of the fluid equals $-f$, where f is the Coriolis parameter, within

each layer, regardless of the thickness of the layer. In our study, the balance between relative vorticity and $-f$ is only a local approximation, valid where the layer depth is small when compared with its basin depth. As the flow moves into deep water the relative vorticity becomes small relative to f. In the Dalziel/Riemenschneider models the balance is global and strong motions in the lower layer persist even where it becomes very thick. These models produce upstream states that are fundamentally different than ours and this leads to differences in distinction between maximal and submaximal states. Potential vorticity is conserved in all models, but the exact value of potential vorticity is not taken to be zero in our model.

One of the main difficulties in discussing two-layer hydraulic models is that the algebra can become quite involved. The situation is exacerbated by the variety of ways that the two layers can become detached from the channel sidewalls, a situation that requires considerable bookkeeping. Riemenschneider et al. (2005, manuscript submitted to *J. Fluid Mech.*) make use of a velocity space, analogous to Armi's (1986) Froude number plane, to present their results. The result is elegant in that the downstream evolution of solutions with various upstream conditions can be followed in a single diagram, but the method requires that the channel width and bottom elevation vary together in a particular way. In our presentation, it is assumed that variations in bottom elevation occur within the straight section of channel and that width changes occur in the basins, where the depth is large and the bottom horizontal. Our description of the maximal and submaximal flow, with all their detached and attached permutations, contains more information than some readers may wish to digest. Such readers should read sections 2 and 3, which describe the basic model and approximations and the algebraically simple case of attached flow at the sill. The same reader could skim through sections 4 and 5, which describe singly and doubly detached flow at the sill, pausing to examine Fig. 4. The material in section 6, which covers the upstream states and maximal and submaximal flows, is crucial (particularly the descriptions of Figs. 9, 10, and 13). The figures skipped as a result of this approach, though not essential to a cursory understanding of the problem, contain information that may save future investigators a great deal of work. A summary of the submaximal and maximal states appears in section 6e and Figs. 15, 16, and 17. Section 7 describes an application to the Strait of Gibraltar. We show that the width of the Atlantic Ocean boundary current along the southern Mediterranean shore serves as an indicator of maximal versus submaximal conditions in the strait. Using a space shuttle photograph that shows the boundary current separation and width, conditions in the Strait at the time of the photograph are evaluated.

2. Governing equations

Consider a rectangular channel separating two relatively wide and deep basins with horizontal bottoms. An exchange flow between the basins could be established as a result of a lock exchange experiment in which the basins are filled with fluids of densities ρ_1 and ρ_2 and are separated by a dam that sits atop the sill (Fig. 1a). The channel has bottom elevation $h^*(y^*)$ and uniform width w^* (dimensional variables are given an asterisk superscript). A rigid lid is placed at $z^* = z_T^*$ and d_1^* and d_2^* are the thicknesses of the upper and lower layers, respectively. Hence,

$$z_T^* = d_1^*(x^*, y^*) + d_2^*(x^*, y^*) + h^*(y^*). \tag{1}$$

The density difference between the two flowing layers is taken to be relatively small and the Boussinesq approximation is employed. The channel is aligned in the y direction and $h^*(y^*)$ and flow properties are assumed to vary gradually with y^*. Scaling suggests the shallow-water equations apply; we do not consider nonhydrostatic effects. Hence, the along-channel velocity v_i^* ($i = 1, 2$ denotes the upper and lower layers) is geostrophic and the corresponding thermal wind relation is

$$f(v_1^* - v_2^*) = -g' \frac{\partial d_2^*}{\partial x^*}, \tag{2}$$

where $g' = g(\rho_2 - \rho_1)/\rho_2$ is the reduced gravity. The cross-channel velocity u_i^* is not generally geostrophic. If the flow is steady, the Bernoulli functions

$$B_1 = \frac{1}{2}[(u_1^*)^2 + (v_1^*)^2] + \frac{p_T^*}{\bar{\rho}} \tag{3}$$

and

$$B_2 = \frac{1}{2}[(u_2^*)^2 + (v_2^*)^2] + \frac{p_T^*}{\bar{\rho}} + g'(d_2^* + h^*) \tag{4}$$

are conserved along streamlines of the respective layers, where p_T^* is the pressure at $z^* = z_T^*$.

The initial layer depths in the downstream and upstream reservoirs are denoted $D_{1\infty}$ and $D_{2\infty}$, each a constant. Once the dam is removed, assuming the flow remains free of dissipation, the potential vorticity of the two layers remains fixed at the uniform values $f/D_{1\infty}$ and $f/D_{2\infty}$. Under the condition of gradual variations along the channel axis the potential vorticity is approximated by $(f + \partial v_i^*/\partial x^*)/d_i^*$ and therefore

$$f + \frac{\partial v_i^*}{\partial x^*} = \frac{f d_i^*}{D_{i\infty}}. \tag{5}$$

In the vicinity of the sill, where $d_i^* \ll D_{i\infty}$, it follows that

$$\frac{\partial v_i^*}{\partial x^*} \simeq -f. \tag{6}$$

Models based on (6) are often referred to under the title "zero potential vorticity" since the relative vorticity exactly equals $-f$ when the potential vorticity of the flow is exactly zero. In the present model, (6) should be regarded as an approximation, valid only where the layer depth d_i^* is small relative to its potential depth $D_{i\infty}$. The dimensional value of the potential vorticity need not be zero.

We introduce the following dimensionless variables

$$x = \frac{x^* f}{\sqrt{g' D_s}}, \quad y = \frac{y^*}{L}, \quad z = \frac{z^*}{D_s}, \quad v_i = \frac{v_i^*}{\sqrt{g' D_s}},$$

and

$$u_i = \frac{fL}{g' D_s} u_i^*, \tag{7}$$

where D_s is the channel depth at the crest of the sill and L is an along-channel length scale. The cross-channel coordinate is nondimensionalized by the local Rossby radius of deformation at the sill section $\sqrt{g' D_s}/f$, as is the channel width w^*. The layer depths d_i^* and bottom topography h^* are nondimensionalized by D_s. In terms of these scales, the dimensionless versions of (2) and (6) are

$$v_2 - v_1 = \frac{\partial d_2}{\partial x} \tag{8}$$

and

$$\frac{\partial v_i}{\partial x} = -1. \tag{9}$$

An important consequence of the limiting case $d_i^* \ll D_{i\infty}$ is that the internal Bernoulli function for the two-layer flow becomes uniform. This result can be deduced from Crocco's relation $dB_i^*/d\psi_i^* = f/D_{i\infty}$ as applied to steady layered flow with Bernoulli function B_i^*, streamfunction ψ_i^*, and uniform potential vorticity $f/D_{i\infty}$ in layer i. The dimensionless form of this relation is $dB_i/d\psi_i = D_s/D_{i\infty}$ ($\ll 1$). Thus B_1, B_2, and therefore the "internal" Bernoulli functions

$$\Delta B = B_2 - B_1 = \frac{1}{2}(v_2^2 - v_1^2) + d_2 + h \tag{10}$$

are all uniform.

Equations (8) and (9) are solved depending on whether the interface between the two layers is attached to both channel sidewalls (section 3), as shown in Fig. 2a, or whether it has detached from one sidewall (section 4) and intersects the channel bottom or top, as shown in Figs. 2b and 2c. We refer to this case as singly detached since a doubly detached configuration (section 5) is also possible, whereby the interface between the two layers intersects both $z = z_T$ and $z = 0$, as shown in Fig. 2d. The separate cases of attachment and detachment result from the assumption of a rectangular channel cross section. Natural straits have a smoothly varying topography, but this introduces difficulties more serious than the bookkeeping required under rectangular geometry.

We will be making frequent use of Gill's (1977) method for deriving conditions for hydraulic criticality. As originally formulated the method assumes that the flow state at any section y of the channel can be described by a single flow variable [$\gamma(y)$, say] that can be linked to the local values of the topographic variables (here the channel width w and depth d) by an algebraic relation of the form $G[\gamma(y); d(y), w(y)] = 0$. The functional G also depends on the upstream conditions, but this dependence is hidden. For fixed upstream conditions, there is typically more than one value of γ that satisfies $G = 0$ at any y. Merger of two such roots occurs where

$$\frac{\partial G}{\partial \gamma} = 0, \tag{11}$$

and this is the condition for hydraulic criticality. To insure that the flow passing through a critical section remain smooth, the regularity condition

$$\frac{\partial G}{\partial h}\frac{dh}{dy} + \frac{\partial G}{\partial w}\frac{dw}{dy} = 0 \tag{12}$$

must also be satisfied here. This condition can restrict the location at which critical flow can occur.

Under conditions of flow separation it becomes difficult to reduce the algebraic problem for two-layer flow to a single equation. We are instead faced with multiple relationships

$$G_i(\gamma_1, \gamma_2, \ldots \gamma_N; d, w) = 0 \quad (i = 1, 2, \ldots N) \tag{13}$$

for dependent variables $\gamma_1, \gamma_2, \ldots \gamma_N$. For the cases encountered later on, $N = 3$. As shown by Pratt and Helfrich (2005), the condition of hydraulic criticality for such systems is given in terms of the generalized Jacobian of the functions G_i as

$$\det\left(\frac{\partial G_i}{\partial \gamma_j}\right)^{\mathrm{T}} = \det\begin{pmatrix} \partial G_1/\partial\gamma_1 & \cdot & \cdot & \partial G_1/\partial\gamma_N \\ \cdot & \cdot & \cdot & \cdot \\ \cdot & \cdot & \cdot & \cdot \\ \partial G_N/\partial\gamma_1 & \cdot & \cdot & \partial G_N/\partial\gamma_N \end{pmatrix} = 0. \tag{14}$$

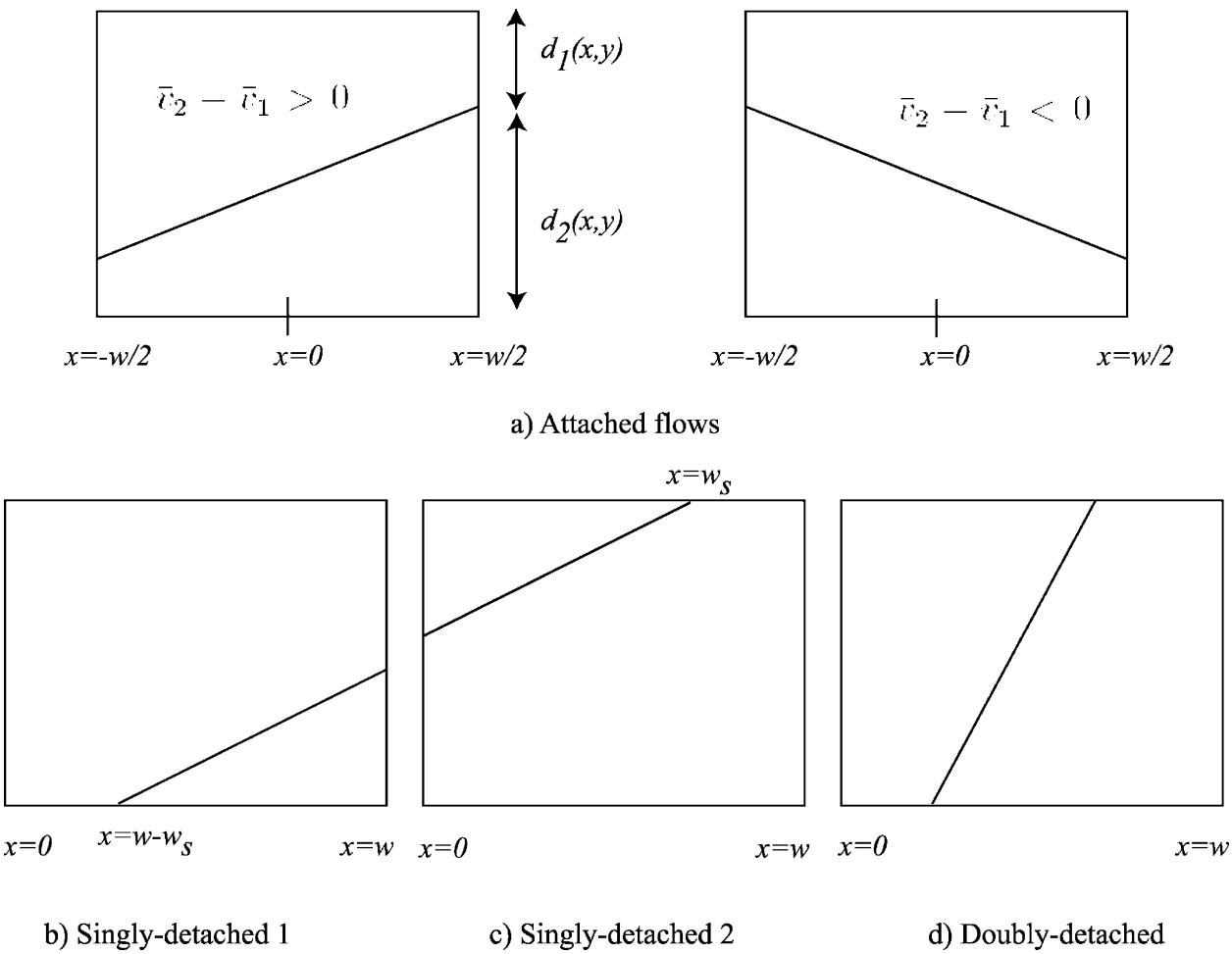

FIG. 2. Channel cross section showing the interface between the two flowing layers at the position of the sill facing the downstream basin.

The corresponding regularity condition is

$$\det\left[\left(\frac{\partial G_i}{\partial \gamma_j}\right)^{\mathrm{T}}\middle|\left(\frac{\partial G_i}{\partial y}\right)_{\gamma}^{\mathrm{T}}\right] = 0, \tag{15}$$

where $[(\partial G_i/\partial \gamma_j)^T|(\partial G_i/\partial y)_\gamma^T]$ is the matrix obtained by replacing the ith column of $(\partial G_i/\partial \gamma_j)^{\mathrm{T}}$ by

$$\left(\frac{\partial G_i}{\partial y}\right)_{\gamma}^{\mathrm{T}} = \begin{bmatrix} (\partial G_1/\partial y)_\gamma \\ (\partial G_2/\partial y)_\gamma \\ \cdot \\ \cdot \\ \cdot \\ (\partial G_N/\partial y)_\gamma \end{bmatrix},$$

and where $(\partial G_i/\partial y)_\gamma$ denotes a derivative with $\gamma_1, \gamma_2, \ldots, \gamma_N$ all held constant.

3. Attached flow at the sill

With the channel spanning $-w/2 < x < w/2$ the solutions to (8) and (9) can be written as

$$v_i(x, y) = -x + \bar{v}_i(y), \tag{16}$$

$$d_1(x, y) = [d(y) - \bar{d}_2(y)] + [\bar{v}_1(y) - \bar{v}_2(y)]x, \tag{17}$$

and

$$d_2(x, y) = \bar{d}_2(y) - [\bar{v}_1(y) - \bar{v}_2(y)]x, \tag{18}$$

where $d = d_1 + d_2$ is the channel depth and the overbars denote the value of the quantity at the center of the channel $x = 0$. At the sill crest, $d = 1$. Note that from (16), the shear, or the left side of (8), is constant, which yields a depth profile that is a linear function of x.

The volume fluxes in the top and bottom layers are

denoted Q_1 and Q_2, respectively where $Q_{1,2} = Q^*_{1,2} f/g' D_s^2$. The effect of rotation on the magnitude of the exchange flow $|Q_2 - Q_1|$ in the attached case can be shown by computing the volume transports in each layer using (16)–(18). That is,

$$Q_1 = \int_{-w/2}^{w/2} v_1\, d_1\, dx = \bar{v}_1\, \bar{d}_1 w + (\bar{v}_2 - \bar{v}_1)\frac{w^3}{12} \quad (19)$$

and

$$Q_2 = \int_{-w/2}^{w/2} v_2\, d_2\, dx = \bar{v}_2\, \bar{d}_2 w - (\bar{v}_2 - \bar{v}_1)\frac{w^3}{12}, \quad (20)$$

or in terms of dimensional variables,

$$Q^*_{1,2} = \bar{v}^*_{1,2}\bar{d}^*_{1,2} w^* \pm (\bar{v}^*_2 - \bar{v}^*_1)\frac{w^{*3} f^2}{12 g'}. \quad (21)$$

In the absence of rotation, the first terms on the right of (19) and (20) would give the layer transport. With rotation, (16) shows how the velocity in each layer decreases as x increases. If $\bar{v}_2 - \bar{v}_1 > 0$, the interface slope is positive and the lower layer is thicker toward the right wall at $x = w/2$, facing downstream. This thicker part on the right has smaller (perhaps even negative) velocities relative to the velocities in the thinner part of the layer to the left. Hence the positive interface tilt reduces the transport in the lower layer. This was pointed out by Dalziel (1990). A similar effect occurs in the upper layer and thus rotation reduces the net exchange $Q_2 - Q_1$. This trend is reminiscent of the tendency of rotation to reduce transports in single-layer overflows. It will be shown later, however, that the tendency is reversed when the two-layer flow becomes doubly detached from the sidewalls.

Attention is restricted to pure exchange flow and we introduce

$$Q = -Q_1 = Q_2 > 0. \quad (22)$$

The formalism of Gill (1977) is used to derive a critical condition at the sill. Begin by combining (22) with (19) and (20), which yields

$$\bar{v}_1(d - \bar{d}_2) = -\bar{v}_2\bar{d}_2, \quad (23)$$

and it follows from (19) that

$$\bar{v}_2 = \frac{(Q/w)(d - \bar{d}_2)}{\bar{d}_2(d - \bar{d}_2) - w^2 d/12} \quad (24)$$

and

$$\bar{v}_1 = \frac{-(Q/w)\bar{d}_2}{\bar{d}_2(d - \bar{d}_2) - w^2 d/12}. \quad (25)$$

To construct a functional G that relates a single dependent variable $\bar{d}_2$ to the parameters that define the channel section, use (16)–(18) to write (10) as

$$\Delta B = \frac{\bar{v}_2^2 - \bar{v}_1^2}{2} + \bar{d}_2 + h. \quad (26)$$

Using (19), (20), and (22) to express (26) in terms of Q leads to

$$G(\bar{d}_2; d, w) = \frac{Q^2 d(d - 2\bar{d}_2)}{2w^2[\bar{d}_2(d - \bar{d}_2) - w^2 d/12]^2} + \bar{d}_2 + h - \Delta B = 0. \quad (27)$$

An equivalent expression was found by Dalziel (1990) [see his (19)]. According to (11), the flow becomes critical where

$$\partial G/\partial \bar{d}_2 = 0. \quad (28)$$

Applying (28) to (27) yields

$$\frac{Q^2}{w^2} = \frac{[\bar{d}_2(d - \bar{d}_2) - w^2 d/12]^3}{d[\bar{d}_2(d - \bar{d}_2) - w^2 d/12 + (d - 2\bar{d}_2)^2]}, \quad (29)$$

which can also be written as

$$\frac{\bar{v}_1^2\bar{d}_2 + \bar{v}_2^2\bar{d}_1 - w^2(\bar{v}_2 - \bar{v}_1)^2/12}{(\bar{d}_1\bar{d}_2 - w^2 d/12)} = 1 \quad (30)$$

if (23) is used. The left side of (30) can be viewed as a Froude number that characterizes the hydraulic state as subcritical, critical, or supercritical for values <1, $=1$, or >1. In the limit of weak rotation ($w \to 0$) it reduces to the familiar composite Froude number

$$\frac{\bar{v}_1^2}{\bar{d}_1} + \frac{\bar{v}_2^2}{\bar{d}_2} (=1 \text{ for critical flow}), \quad (31)$$

as discussed by Armi (1986). Similarly, the left side of (30) could be regarded as the composite Froude number in the rotating case.

The regularity condition (12) can be applied to determine further restrictions on the location of a section of hydraulic control. Attention is confined to the channel portion of the domain, for which w = constant. After use of (29) and some lengthy algebra, (12) reduces to

$$\left[(d - \bar{d}_2)^2 - \frac{w^2 d}{12}\right]\frac{dh}{dy} = 0, \quad (32)$$

which stipulates that the control can occur where $dh/dy = 0$ (as at the sill) or where $\bar{d}_2 = \bar{d}_{2v}$, with

$$\bar{d}_{2v} = d - \frac{w d^{1/2}}{2\sqrt{3}}. \quad (33)$$

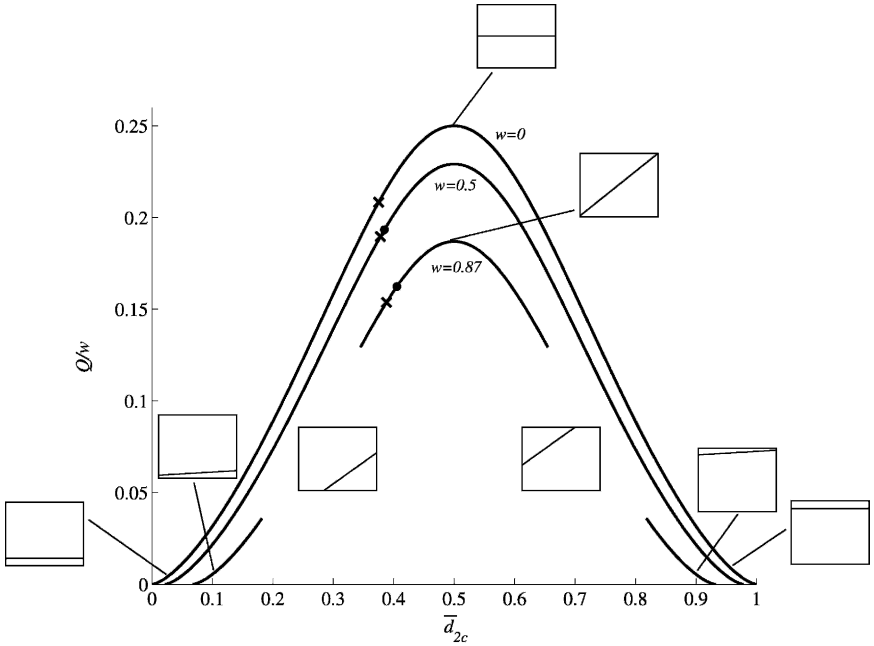

FIG. 3. The exchange flow rate as a function of the depth $\overline{d}_{2c}$ of the bottom layer at the center of the channel for attached flow and critical conditions at the sill crest. The diagrams show the channel cross section at the sill, indicating the interface between the two layers. The crosses on the curves indicate the maximal exchange as derived in section 6. The dots on the curves indicate the exchange flow rate, also derived in section 6, using a virtual control found to lie at some point over the sloping bottom of the channel upstream of the sill.

Locations at which (33) are satisfied are called virtual controls (Wood 1968). In the limit of weak rotation, satisfaction of (33) requires $\overline{d}_{2v} \to d$. As discussed by Armi (1986) the virtual control in this case occurs in the deep reservoir, when the upper layer is thin and the lower layer is infinitely deep and inactive. An interesting aspect of the rotating problem is that the virtual control apparently can exist in shallower reaches of the channel. We will return to this point in section 6, where connection of the sill flow with the upstream basin is discussed. For the time being, attention will be restricted to critical flow at the sill.

If (29) is evaluated at the sill ($d = 1$) the result can be used to plot the exchange transport per unit width Q/w as a function of the critical value of $\overline{d}_2$ (denoted $\overline{d}_{2c}$) for various w, shown in Fig. 3. Figure 3 shows that there are no critical solutions (either attached or detached) as $\overline{d}_{2c} \to 0$ or $\overline{d}_{2c} \to 1$, for moderate values of rotation. As one of the layers becomes very thin while remaining attached, the interface slope $\overline{v}_2 - \overline{v}_1 \to 0$. In the case of no barotropic flow, from (23), this implies that both $\overline{v}_2 = 0$ and $\overline{v}_1 = 0$ for finite d. Hence, from (24) and (25), $Q/w = 0$ for finite $\overline{d}_2$ or $\overline{d}_1$. For fixed $\overline{d}_{2c}$, increases in rotation (increases in $w = w^*f/\sqrt{g'D_s}$) reduce the transport. Note that f does not appear in the scaling for Q/w $[=Q^*/(w^*g'^{1/2}D_s^{3/2})]$. The gaps in the $w = 0.87$ curve are for ranges $0.182 < \overline{d}_2 < 0.345$ and $0.655 < \overline{d}_2 < 0.818$ over which the flow becomes detached from one of the sidewalls, and will be discussed further in section 4. For $w \leq 0.866$, the flow at the sill is always attached to both sidewalls.

For the attached case, critical conditions with $\overline{d}_{2c} = 1/2$ yield the largest value of Q/w. However, it is shown in section 6 that such a flow cannot be connected to an adjacent basin when a sill is present in the channel, and therefore the maximal exchange is less than for $\overline{d}_{2c} = 1/2$.

4. Singly detached flow at the sill

Consider a singly detached exchange flow where the interface between the two layers intersects either $z = z_T$ or $z = 0$. For a positive interface slope ($\overline{v}_2 - \overline{v}_1 \geq 0$), the flow detaches from the right wall ($x = w/2$) when

$$\overline{d}_2 \geq d - (\overline{v}_2 - \overline{v}_1)\frac{w}{2},$$

and it detaches from the left wall ($x = -w/2$) when

$$\overline{d}_2 \leq (\overline{v}_2 - \overline{v}_1)\frac{w}{2},$$

as can be seen from (18). It is convenient in the detached case to shift the channel to lie between $0 < x < w$, as shown in Figs. 2b and 2c.

From (8) and (9), the velocity and depth profiles for the singly detached, positive interface slope case shown in Fig. 2b are found to be

$$v_i(x, y) = w - w_s - x + \hat{v}_i(y), \tag{34}$$

$$d_1(x, y) = \begin{cases} d(y) - \hat{v}_-(x + w_s - w) & (x \geq w - w_s) \\ d(y) & (x < w - w_s) \end{cases}, \tag{35}$$

and

$$d_2(x, y) = \begin{cases} \hat{v}_-(x + w_s - w) & (x \geq w - w_s) \\ 0 & (x < w - w_s) \end{cases}, \tag{36}$$

where the caret over a variable implies its value at $x = w - w_s$, the point where the interface intersects the bottom of the channel $z = 0$, and $\hat{v}_\pm = \hat{v}_2 \pm \hat{v}_1$. The interface remains attached to the right wall $x = w$. The volume fluxes in the two layers are given by

$$Q_2 = \int_{w-w_s}^{w} d_2 v_2 \, dx = w_s^2(\hat{v}_2 - \hat{v}_1)\left(\frac{\hat{v}_2}{2} - \frac{w_s}{3}\right) \tag{37}$$

and

$$Q_1 = \int_0^{w-w_s} d_1 v_1 \, dx + \int_{w-w_s}^{w} d_1 v_1 \, dx = dw\left(\hat{v}_1 - w_s + \frac{w}{2}\right) - w_s^2(\hat{v}_2 - \hat{v}_1)\left(\frac{\hat{v}_1}{2} - \frac{w_s}{3}\right). \tag{38}$$

In the singly detached case 1, the value of the Bernoulli function can be determined by evaluating (10) where the interface intersects the bottom. Thus,

$$\Delta B = \frac{\hat{v}_+\hat{v}_-}{2} + z_T - d. \tag{39}$$

Similar equations can be derived for the singly detached case 2, shown in Fig. 2c.

As in the attached case, the net transport is again assumed to be zero and $Q = -Q_1 = Q_2 > 0$. Unlike in the attached case, it is simpler to use three functionals in place of G for three dependent variables $\hat{v}_\pm = \hat{v}_2 \pm \hat{v}_1$ and w_s. The first functional is found from (39), and the second and third from (37) and (38) as follows:

$$G_1(\hat{v}_-, \hat{v}_+; d) = \hat{v}_+\hat{v}_- - 2(\Delta B - z_T + d) = 0, \tag{40}$$

$$G_2(\hat{v}_-, \hat{v}_+, w_s) = w_s^2\hat{v}_-\left(\frac{\hat{v}_+ + \hat{v}_-}{4} - \frac{w_s}{3}\right) - Q = 0, \tag{41}$$

and

$$G_3(\hat{v}_-, \hat{v}_+, w_s; d, w) = w_s^2\hat{v}_-^2 - dw(\hat{v}_- - \hat{v}_+ - w + 2w_s) = 0. \tag{42}$$

The condition for criticality is obtained by applying (14) with $\gamma_1 = \hat{v}_-$, $\gamma_2 = \hat{v}_+$, and $\gamma_3 = w_s$, leading to

$$\hat{v}_- w_s\{wd(3\hat{v}_+^2 - 6\hat{v}_+ w_s + 4w_s^2) - 6\hat{v}_- wd(-\hat{v}_+ + 2w_s) + \hat{v}_-^2[3wd + 2w_s^2(-3\hat{v}_+ + 4w_s)]\} = 0. \tag{43}$$

If (43) is evaluated at the sill ($d = 1$), the result can be solved simultaneously with (41) and (42) to determine how Q varies with w_s for a given w. The results are indicated by the dashed curves in Fig. 4. The interface is doubly detached to the right of the termination of the dashed curves. That is,

$$d - (\bar{v}_2 - \bar{v}_1)\frac{w}{2} < \bar{d}_2 < (\bar{v}_2 - \bar{v}_1)\frac{w}{2}.$$

For $w < 1.001$, the sill flow remains attached to at least one wall.

The curves in Fig. 4 show that at larger values of w, double separation occurs more readily. Further, the magnitude of the exchange flow increases for a given flow width as rotation increases. However, it will be shown in section 6 that the magnitude of the maximal exchange decreases with increasing rotation if the sill flow is singly detached. Note that by symmetry the plot is the same when the interface intersects the channel top $z = z_T$ and the right wall (Fig. 2c), in which case w_s is interpreted as the width of the upper layer at $z = z_T$.

For a given w, the relationship between Q and w_s is not necessarily unique, and there are two values of w_s having the same Q. The second solutions are indicated by the second set of dashed curves in Fig. 4 for large values of w_s/w. For $w > 1.720$, there is only one solution, while there are two singly detached solutions when $0.866 \leq w \leq 1.720$.

Last, Fig. 5 shows the relationship between $\bar{d}_{2c}$ and Q/w for $w = 0.87$. The curves fill in the gaps in the $w = 0.87$ curves of Fig. 3. The depth $\bar{d}_{2c}$ is defined as d_{2c} ($x = w - w_s/2$) in the case of Fig. 2b and d_{2c} ($x = w_s/2$) in the case of Fig. 2c. The dotted lines correspond to the second solution, where $w_s/w \approx 1$, shown in the lower-right corner of Fig. 4.

5. Doubly detached flow at the sill

We have thus far considered the case where the interface intersects at least one of the channel sidewalls at the sill cross section. Here, we explore doubly detached flows in which the interface between the two flowing layers at the sill intersects both the channel floor $z = 0$ and outcrops at the surface $z = z_T$. The variables are

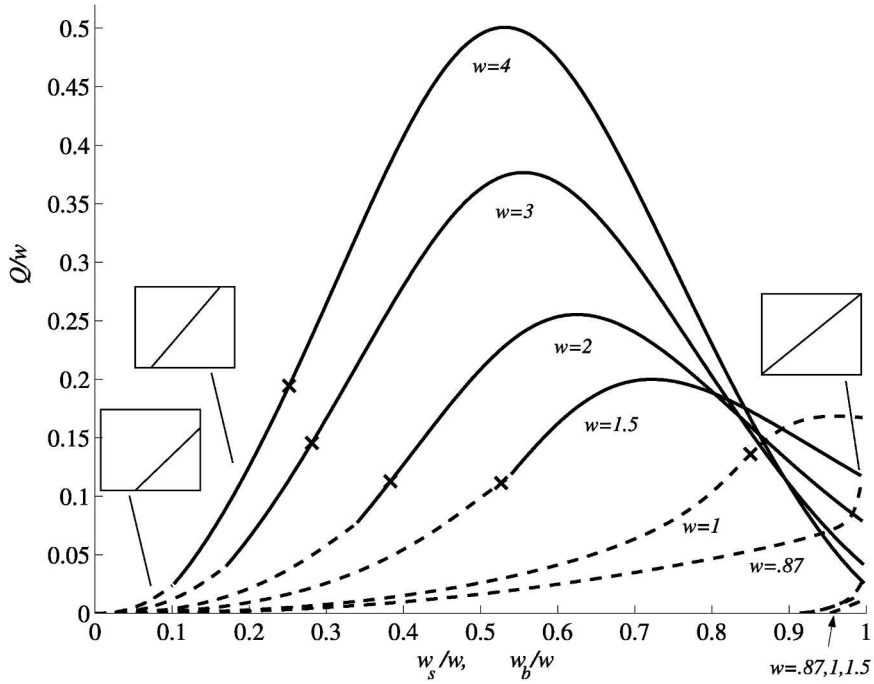

FIG. 4. The exchange flow rate as a function of the width of the singly detached flow (dashed curves) and the doubly detached flow (solid curves) for critical conditions at the sill crest. Crosses on the curves indicate the maximal exchange in terms of w_s as found in section 6.

defined in Fig. 6. The velocity and depth profiles for the doubly detached case shown in Figs. 2d and 6 are

$$v_i(x, y) = w_t - w_b - x + \hat{v}_i(y), \tag{44}$$

$$d_1(x, y) = \begin{cases} d(y) & x < w_t - w_b \\ d(y) - \hat{v}_-(x + w_b - w_t) & w_t - w_b \le x \le w_t \\ 0 & x > w_t \end{cases}, \tag{45}$$

and

$$d_2(x, y) = \begin{cases} 0 & x < w_t - w_b \\ \hat{v}_-(x + w_b - w_t) & w_t - w_b \le x \le w_t \\ d(y) & x > w_t \end{cases}, \tag{46}$$

where the caret over a variable implies its value at the point where the interface intersects the channel bottom $z = 0$, $x = w_t - w_b$ (as before, $\hat{v}_\pm = \hat{v}_2 \pm \hat{v}_1$). The volume fluxes in the two layers are given by

$$Q_1 = \int_0^{w_t - w_b} dv_1\, dx + \int_{w_t - w_b}^{w_t} d_1 v_1\, dx = dw_t\left(\frac{w_t}{2} - w_b + \hat{v}_1\right) + \hat{v}_- w_b^2\left(\frac{w_b}{3} - \frac{\hat{v}_1}{2}\right) \tag{47}$$

and

$$Q_2 = \int_{w_t - w_b}^{w_t} d_2 v_2\, dx + \int_{w_t}^{w} dv_2\, dx = d(w - w_t)\left(\frac{w_t - w}{2} - w_b + \hat{v}_2\right) - \hat{v}_- w_b^2\left(\frac{w_b}{3} - \frac{\hat{v}_2}{2}\right). \tag{48}$$

Note that

$$w_b = \frac{d}{\hat{v}_-} \tag{49}$$

for finite rotation and within the limits of the definition of w_b. This can be used to eliminate w_b from (47) and (48). The value of ΔB can be determined by evaluating (10) where the interface intersects the bottom, leading to

$$\Delta B = \frac{\hat{v}_+ \hat{v}_-}{2} + z_T - d. \tag{50}$$

It is again assumed that the net transport is zero $Q = -Q_1 = Q_2 > 0$ and the critical condition for doubly detached sill flow is derived. As in the singly detached case, three functionals for three dependent variables $\hat{v}_\pm = \hat{v}_2 \pm \hat{v}_1$ and w_t are used. The first functional is found

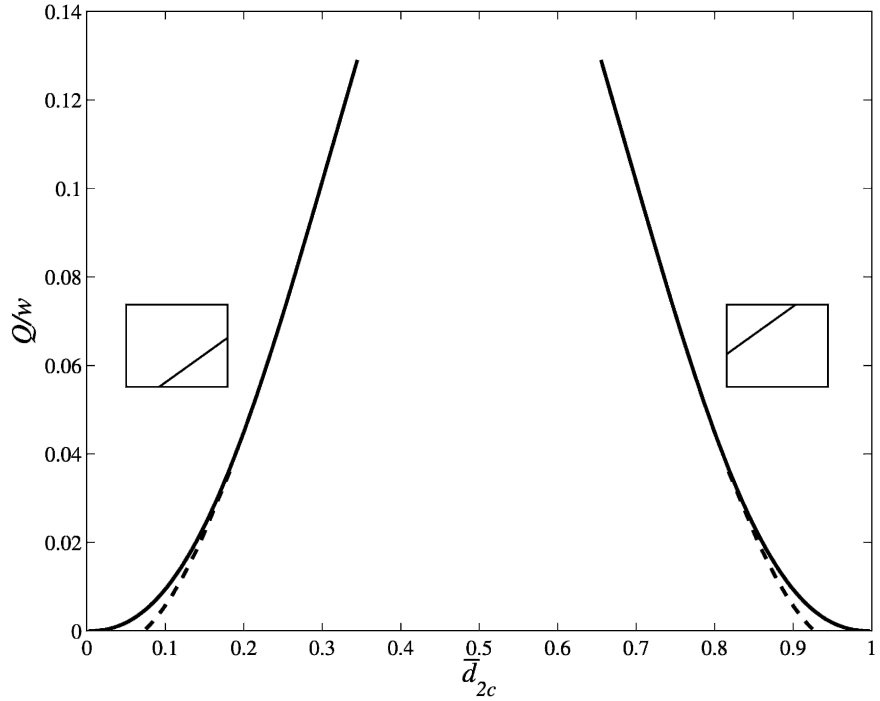

FIG. 5. The exchange flow rate as a function of the depth at the center of the singly detached bottom layer for critical conditions at the sill crest and $w = 0.87$.

from (50), and the second and third from (47) and (48) as follows:

$$G_1(\hat{v}_-, \hat{v}_+; d) = \hat{v}_+\hat{v}_- - 2(\Delta B - z_T + d) = 0, \tag{51}$$

$$G_2(\hat{v}_-, \hat{v}_+, w_t; d) = dw_t\hat{v}_-[w_t\hat{v}_- - 2d + \hat{v}_-(\hat{v}_+ - \hat{v}_-)] + d^2\left[\frac{2d}{3} - \frac{(\hat{v}_+ - \hat{v}_-)}{2}\hat{v}_-\right] + 2Q\hat{v}_-^2 = 0, \quad \text{and} \tag{52}$$

$$G_3(\hat{v}_-, \hat{v}_+, w_t; d, w) = \hat{v}_-^2(2w_t - w) + \hat{v}_-(w^2 - 2ww_t - d - \hat{v}_+w) + 2\,dw = 0. \tag{53}$$

Applying (14) with $\gamma_1 = \hat{v}_-$, $\gamma_2 = \hat{v}_+$, and $\gamma_3 = w_t$ the criticality condition is found to be

$$\hat{v}_-^2\{\hat{v}_-dw^2(\hat{v}_+ - \hat{v}_- + 2w_t) - \hat{v}_-d^2[\hat{v}_- + \hat{v}_+ + 6(w_t - w)] + 8Q\hat{v}_-(w - \hat{v}_-) + 2d^2(d - w^2) + 2\hat{v}_-^2d[w_t(\hat{v}_+ + \hat{v}_-) - w(\hat{v}_+ - \hat{v}_-) + 2w_t(w_t - 2w)]\} = 0. \tag{54}$$

Equations (52), (53), and (54) can now be solved simultaneously to determine how Q varies with w_t (or w_b) for a given geometry, as shown by the solid curves in Fig. 4. Because of symmetry, the curves are equivalent to those if w_s ($= w + w_b - w_t$) had been plotted. Critical sill flow may be doubly detached for $w \geq 1.001$. As in the singly detached case, the magnitude of the exchange flow increases for a given flow width as the effect of rotation increases. However, in section 6, we show that, unlike in the singly detached case, the maxi-

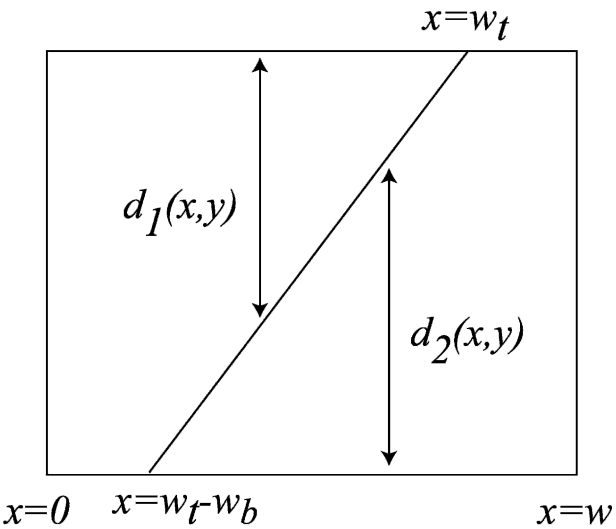

FIG. 6. Channel cross section showing the doubly detached interface between the two flowing layers facing the downstream basin.

mal states that are doubly detached at the sill in fact have increasing volume fluxes for increasing rotation.

The regularity conditions for singly and doubly detached flow are considerably more complicated than that for the attached case. In addition to channel sections with $dh/dy = 0$ critical flow can occur over a sloping bottom provided a regularity condition is satisfied there. The corresponding expressions are given in the appendix.

6. Connecting the sill flow to the basin

a. Maximal and submaximal exchange

It has been shown how distinct flow configurations at the sill can be derived. The requirement of dynamically connecting the sill flow to the flow in an adjacent basin determines which sill flows are allowable. Farmer and Armi (1986) use Froude number diagrams of the analogous nonrotating two-layer flow to investigate possible solutions and to derive the maximal exchange solutions between two infinitely wide or deep basins connected by a channel of uniform width w containing a sill. They show that the requirement for the constant volume flux $Q = Q_2 = -Q_1$ to be maximal for a given geometry is that the flow is critical both at the sill crest and at the mouth of the channel (the entrance to the upstream basin). The flow is then subcritical between these two critical control sections and supercritical on either side. In this way, the *maximal* exchange state is that which is isolated from the upstream and downstream basins. *Submaximal* exchange, for which there exists only one control section, has subcritical upstream flow in both the channel and the basin.

The presence of rotation leads to a more complex assortment of possible basin states. One view of the upstream circulation is guided by a reasonable expectation of the outcome of the lock exchange problem suggested in Fig. 1a. When the barrier is removed, the deep layer will spill over the sill and a shallow reverse flow will form above. As this reverse flow moves into the upstream basin, it overrides a lower layer that becomes progressively deeper and presumably more quiescent. The upper layer itself remains shallow and therefore subject to (6). In the deeper layer, the depth d_2^* is no longer $\ll D_{2\infty}$ and (6) is replaced by the condition

$$f + \frac{\partial v_2^*}{\partial x^*} = \frac{f d_2^*}{D_{2\infty}}. \tag{55}$$

As the basin is approached, $d_2^* \to D_{2\infty}$ and $\partial v_2^*/\partial x^* \to 0$. The surface current now rides over a lower layer that is essentially inactive. As the channel widens into the basin it is quite possible that the surface flow will detach from the right wall and form a boundary current of dimensionless width w_e. The structure of this current can be determined by requiring that its energy and volume transport be the same as at the sill. It must be acknowledged, however, that the whole scenario is hypothetical and must ultimately be verified by performing the lock exchange experiment.

Based on nonrotating examples such as Armi (1986) and on the findings of Dalziel (1990) and Riemenschneider et al. (2005, manuscript submitted to *J. Fluid Mech.*), both of which concentrate on cases of moderate to low rotation, we expect to find for each w a family of submaximal solutions with a limiting maximal solution. The submaximal solutions will have a single hydraulic control at the sill with subcritical flow at all points upstream; the maximal solution will have a sill control, subcritical flow extending a finite distance upstream and terminating in a second control, and supercritical flow upstream of this, perhaps terminating in a hydraulic jump. Within the context of our model, which has different upstream conditions than the previous two studies, there are two possible locations for the second control. The first is at the channel mouth, where the straight section of channel ends and the total depth is effectively infinite. By hypothesis the lower layer at this section is inactive and the thin upper layer is therefore unforced. The regularity condition for critical flow is simply $dw/dy = 0$, which is satisfied just inside the mouth. This type of control, which is analogous to Armi's "exit" control, is our preferred mode of upstream critical flow. Maximal flows can be found by requiring that the mouth flow be critical and have the same volume flux and energy as the critical sill flow.

A second possibility is that the upstream control is a "virtual control" satisfying the regularity condition (12) or (15). The specific constraint for attached flow is given by (33) and the appendix lists the corresponding formulas for singly and doubly detached flows. In contrast to an exit control, the virtual control can occur in those parts of the channel where the depth is finite and the bottom slope is nonzero. In his Ph.D. thesis, Dalziel (1988) alludes to controls of this type but remarks only that the regularity condition "fails to yield any solutions in the range of interest." Riemenschneider (2004) and Riemenschneider et al. (2005, manuscript submitted to *J. Fluid Mech.*) describe specific solutions with virtual controls. In none of these studies is the regularity condition itself written down. However, Riemenschneider (2004) notes that the position of the virtual control moves from upstream into shallower water and closer to the sill as w increases, and this is borne out by our

(33). Her calculations with virtual controls are confined to flows that are attached at the sill and upstream.

We have considered the possibility that virtual controls arise in our model. For each critical sill flow, we check to see whether there is a second upstream section of critical flow with the same volume transport and energy and for which the regularity condition [(33), or its versions for detached flow] is satisfied. The meaning of the exercise is not completely clear for small values of w since the virtual control tends to occur in deep water, just where the zero potential vorticity equations themselves are expected to fail. However, for moderate values of w and attached sill flow we do find virtual controls that lie in shallower reaches of the channel and that are consistent with those found by Riemenschneider (2004). The maximal flux in each case is larger, but only slightly so, than the maximal flux found with an exit control for the same w (see the dots in Fig. 3). Moreover, physically meaningful mouth states for the case with virtual controls cannot be found; that is, the flow at the virtual control cannot be continued into the channel mouth under the conditions of an inactive lower layer at the mouth. In addition, virtual controls are not found for any cases in which the sill flow is singly or doubly detached. We have therefore elected to reject the virtual control scenario and hold fast with the hypothesis of an exit control.

As suggested in Fig. 1b the "mouth" is located where the straight section of channel terminates and the channel begins to broaden. The channel width in the broadening region is denoted $w_B(y)$ and $w_B = w$ at the mouth. The flow in the broadening region can either be attached to both channel walls or detached from one wall. If the mouth flow is attached, and the channel center is taken to be at $x = 0$, the upper-layer velocity and depth profile in the mouth are found from the governing Eqs. (8) and (9) with $v_2 = 0$,

$$v_1(x) = \frac{2\hat{d}}{w_B} - x, \quad \text{and} \tag{56}$$

$$d_1(x) = \overline{d} + \frac{2\hat{d}x}{w_B} - \frac{x^2 - (w_B/2)^2}{2}, \tag{57}$$

where

$$\overline{d} = \frac{1}{2}(d_1|_{w_B/2} + d_1|_{-w_B/2}), \tag{58}$$

$$\hat{d} = \frac{1}{2}(d_1|_{w_B/2} - d_1|_{-w_B/2}), \tag{59}$$

and the sidewalls are at $x = \pm w_B/2$. The volume exchange flux is given by

$$Q = -\int_{-w_B/2}^{w_B/2} v_1\, d_1\, dx = -2\hat{d}\overline{d}. \tag{60}$$

Using (56) and (57) in (10), the internal Bernoulli function is found to be

$$\Delta B = -\frac{2\hat{d}^2}{w_B^2} - \frac{w_B^2}{8} - \overline{d} + z_T. \tag{61}$$

If the mouth flow is detached from the right wall, it is convenient to shift the channel coordinates to run from $x = 0$ to $x = w$ at the mouth. The upper-layer velocity and detached parabolic depth profile [from (8) and (9) with $v_2 = 0$] are then

$$v_1(x) = v_0 - x \tag{62}$$

and

$$d_1(x) = v_0 x - \frac{x^2}{2} + d_0, \tag{63}$$

where v_0 and d_0 are the velocity and depth at the wall $x = 0$. Using these in (10) yields

$$\Delta B = -\frac{v_0^2}{2} + z_T - d_0. \tag{64}$$

The exchange transport is the magnitude of the geostrophic flux in the active layer

$$Q = -\int_0^{w_e} v_1\, d_1\, dx = \frac{d_0^2}{2}, \tag{65}$$

where w_e is the width of the surface flow (at the mouth, $w_e \le w$) and using $d_1(x = w_e) = 0$. This condition also gives

$$v_0 = \frac{w_e}{2} - \frac{(2Q)^{1/2}}{w_e}. \tag{66}$$

Figure 7 shows the three forms that the boundary current can take. Supercritical flow, shown in Fig. 7a, occurs when the layer thickness is maximum at $x = 0$ and v_1 is everywhere toward the upstream basin. As shown by Stern (1980), critical flow (Fig. 7b) occurs when the interface slope is zero on the left wall at $x = 0$ and therefore $v_1 = 0$. If the current thickness d_1 reaches a maximum to the right of the wall at $x = 0$ (Fig. 7c), then in the region between $x = 0$ and the maximum thickness the current is flowing toward the downstream basin. To the right of the maximum thickness, where $v_1 = 0$, the current flows upstream. This configuration is subcritical. The only net transport occurs in the shaded region. Note that this subcritical flow has the same Q as the supercritical flow in Fig. 7a because both flows have the same d_0. For any subcritical flow, there exists a supercritical flow having the same v_0, d_0, and Bernoulli function.

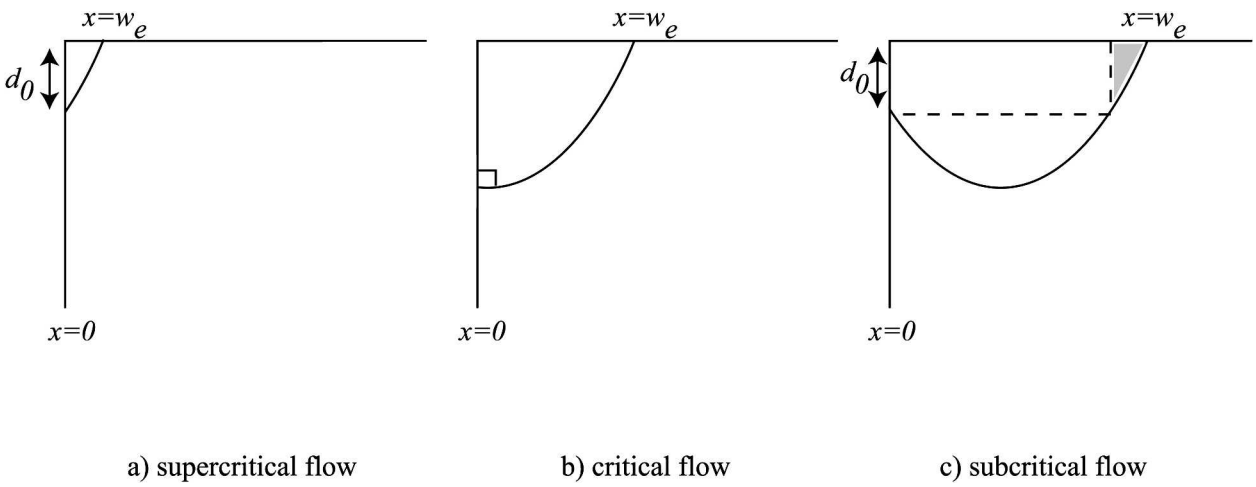

FIG. 7. Detached buoyant flow in the mouth or upstream basin, drawn facing the downstream basin. The width of the surface boundary flow is w_e.

b. Attached sill flow

1) CONNECTION TO THE MOUTH

Attached sill flows may be either attached or detached at the mouth. Attached mouth flows are considered first. The internal Bernoulli function at the sill for critical, attached flow is, from (27), given by

$$\Delta B = \frac{Q^2(1 - 2\overline{d}_{2c})}{2w^2[\overline{d}_{2c}(1 - \overline{d}_{2c}) - w^2/12]^2} + \overline{d}_{2c} + (z_T - 1). \tag{67}$$

Recall that ΔB is uniform across the width of the flow, thus the resulting condition between $\overline{d}$ and $\overline{d}_{2c}$ is found by equating (61) and (67):

$$\overline{d}^3 + \overline{d}^2\left\{\frac{Q^2(1 - 2\overline{d}_{2c})}{2w^2[\overline{d}_{2c}(1 - \overline{d}_{2c}) - w^2/12]^2} + \overline{d}_{2c} - 1 + \frac{w_B^2}{8}\right\} + \frac{Q^2}{2w_B^2} = 0, \tag{68}$$

where $\overline{d}_{2c}$ is related to Q by (29). Further, (60) has been used to eliminate $\hat{d}$.

For a given w (and taking $w_B = w$), subcritical and supercritical solutions for $\overline{d}$ exist only over a restricted range of $\overline{d}_{2c}$ values so that only some critical flows can be associated with an attached flow in the mouth, as shown in Fig. 8. Subcritical and supercritical roots coalesce as some value $\overline{d}_{2c} = \overline{d}^c_{2c}$ is approached. This is the point where conditions in the mouth are also critical and Q/w is a maximum for a given geometry.

In the limiting case of zero rotation ($w \ll 1$), subcritical and supercritical solutions for $\overline{d}$ coalesce where $\overline{d}^c_{2c} = 0.375$ (Fig. 8), corresponding to maximal exchange. This maximal exchange state was derived by Farmer and Armi (1986) for nonrotating flow over a sill. The corresponding maximal value of Q/w is marked by a cross on the $w = 0$ curve in Fig. 3.

As the upper layer moves into the widening upstream basin, it eventually detaches from the right wall, and at this point $\hat{d} = -\overline{d}$ since $d_1|_{x=w_e/2} = 0$, where w_e is the width at some point upstream of the mouth for which the flow detaches. This width is found by solving (60) and (68), while increasing $w_B(y)$. Subcritical basin currents associated with submaximal solutions detach for $2\sqrt{2} \geq w_e > 2.05$ corresponding to $0 \leq \overline{d}_{2c} < 0.375$ and $0 \leq Q/w < 0.207$. The dynamics of such a detached boundary current in the upstream basin will be discussed in the next section.

For moderate rotation $w = 0.5$, for which the sill flow remains attached, solutions at the mouth can be found in the range $0.021 \leq \overline{d}_{2c} \leq 0.378$. As discussed previously, there are no solutions for $\overline{d}_{2c} < 0.021$. The maximum $\overline{d}^c_{2c} = 0.378$ corresponds to the maximal flow $Q/w = 0.190$. The corresponding critical flow at the mouth is supercritical in the basin and detachment from the right wall occurs where $w_e = 0.6$. The subcritical basin currents associated with submaximal solutions detach for $2.80 \geq w_e > 1.45$.

As rotation strengthens, the situation is complicated by the fact that the flow may become detached at the sill. For $w \leq 0.881$, maximal flow occurs when the sill flow is attached. For $w = 0.87$, maximal flow occurs when $\overline{d}^c_{2c} = 0.388$ and $Q/w = 0.155$. The associated mouth flow, which is attached, becomes supercritical as the channel widens into the basin and detaches at $w_e = 0.9$. The subcritical basin currents associated with submaximal solutions detach for $1.44 \geq w_e \geq 1.15$ (corre-

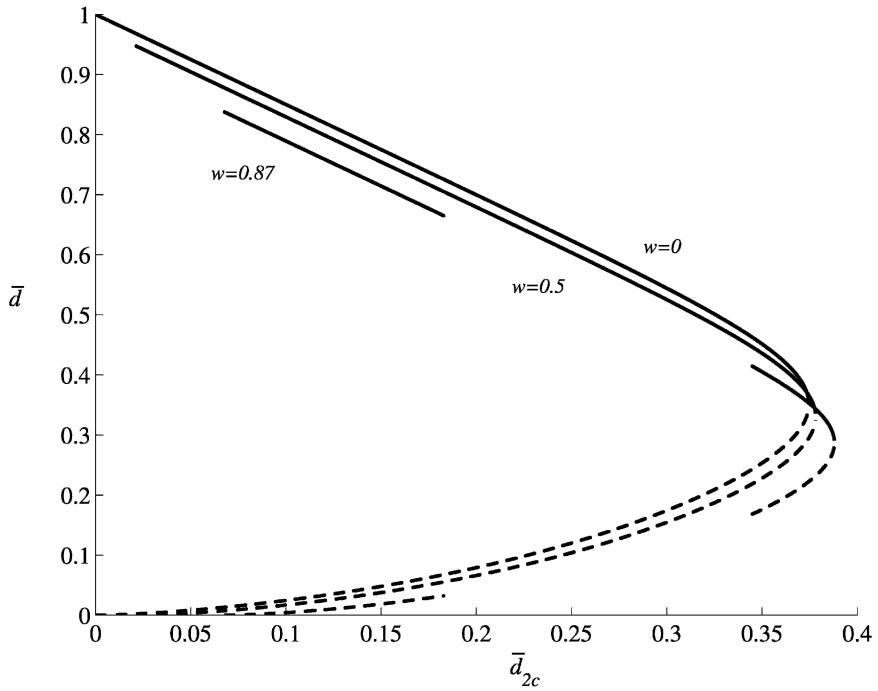

FIG. 8. The mean depth of the attached mouth flow corresponding to the depth of the lower layer at the center of the channel for attached flow and critical conditions at the sill crest. Critical flow occurs at the mouth, corresponding to maximal exchange, when subcritical solutions (solid curves) and supercritical solutions (dashed curves) coalesce.

sponding to $0.350 \leq \overline{d}_{2c} < 0.388$). The subcritical flows corresponding to the range $0.068 \leq \overline{d}_{2c} \leq 0.183$ detach for $2.73 \geq w_e \geq 2.24$. Detached sill flow where $0.183 < \overline{d}_{2c} < 0.350$ is explored in section 6c.

It has been shown how the solutions on the right side of Fig. 3 (corresponding to a thicker lower layer as shown in the inset channel cross sections) have been eliminated. Only those solutions having $\overline{d}_{2c} \leq \overline{d}^{c}_{2c}$ are realizable since all other solutions cannot be linked to flow at the mouth.

2) CONNECTION TO THE UPSTREAM BASIN

There is no constraint on the width w_e of the surface flow in the wide upstream basin. The constant internal Bernoulli function is given by (64) and the exchange transport by (65). The Bernoulli functions, (67) and (64), for the attached flow at the sill and the flow in the basin are equated to find a relationship between Q and w_e,

$$\left[\frac{w_e}{2} + \frac{(2Q)^{1/2}}{w_e}\right]^2 = 2 - 2\overline{d}_{2c} - \frac{Q^2(1 - 2\overline{d}_{2c})}{w^2[\overline{d}_{2c}(1 - \overline{d}_{2c}) - w^2/12]^2}, \quad (69)$$

where $\overline{d}_{2c}$ is again related to Q by the critical condition (29). Solutions to (69) and (29) yield a type of "weir" relation in which Q/w is given in terms of w_e (Fig. 9). Solutions for $w = 0.5, 0.87$, where the flow is detached at the mouth are included in this figure. Note from Fig. 9 that in some cases several Q/w are possible for the same w_e; this is true, for example, in the case of $w = 0.5$. Although all of the detached basin currents indicated in Fig. 9 can be matched to sill flows with the same Q and ΔB, they cannot all be so matched to mouth flows. Allowable states, meaning those that can be matched at all three locations, are indicated as thick curves. If attention is restricted to the latter, the relationship between Q/w and w_e for given w becomes unique.

In the limit of zero rotation $w \ll 1$, the critical sill flow maintains finite Q/w and therefore $Q \ll 1$. It can be shown directly from (69) that the supercritical root w_e in this limit is $O(Q)^{1/2} \ll 1$, while the subcritical root is $O(1)$. The thick portions of the $w \ll 1$ curve in Fig. 9, indicating the realizable subcritical flows, show the previous findings that subcritical basin currents associated with submaximal solutions detach at values ranging from $w_e = 2.05$ to $w_e = 2\sqrt{2}$.

For $w = 0.5$, supercritical and subcritical upstream states are found starting from the minimum value $\overline{d}_{2c} = 0.021$. Similarly for $w = 0.87$. A plan view of maximal

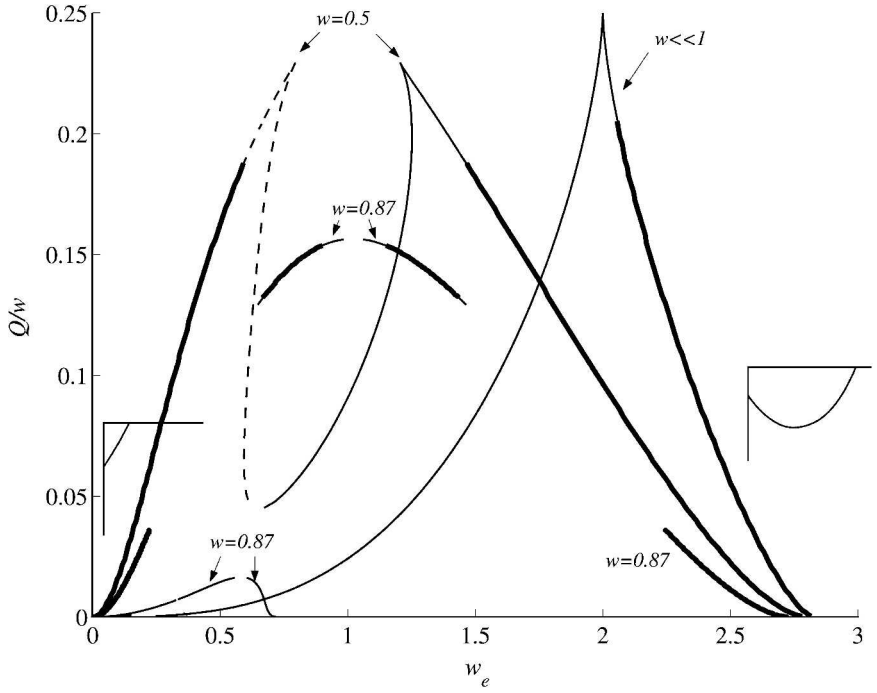

FIG. 9. Exchange flow rate as a function of the width w_e of the current in the upstream basin for critical and attached conditions at the sill crest. The singly detached mouth states are also included in this figure. The realizable flows, shown by the thick curves, are those that can be dynamically connected from the sill to the mouth and basin with the same exchange flux and Bernoulli function.

and submaximal exchange flows for $w = 0.5$ is shown in Fig. 10. A further effect to note is the recirculation in the upstream subcritical flow. Some such recirculations can be attributed to the geometry of the mouth. For example, Bormans and Garrett (1989a) suggest that a key parameter determining whether the exit flow from a strait forms a gyre or a coastal jet is the sharpness of the exit corner relative to the inertial radius u/f. Our model appears to produce a counterexample in that no minimum curvature at the mouth is required to produce a band of reverse flow. This feature is discussed in the context of the Strait of Gibraltar in section 7.

c. *Singly detached sill flow*

We consider the case where the sill flow is detached from one wall and we match it to upstream flow that can be either attached or detached at the mouth, again by equating sill and mouth Bernoulli functions. No physical solutions for any value of w are found for the singly detached flows shown in Fig. 2c. Singly detached sill flows that outcrop at the surface cannot be linked to any mouth flow (either attached or detached), and we conclude that such flows cannot exist. The analysis that follows is for the singly detached sill flows that intersect the channel floor, as shown in Fig. 2b.

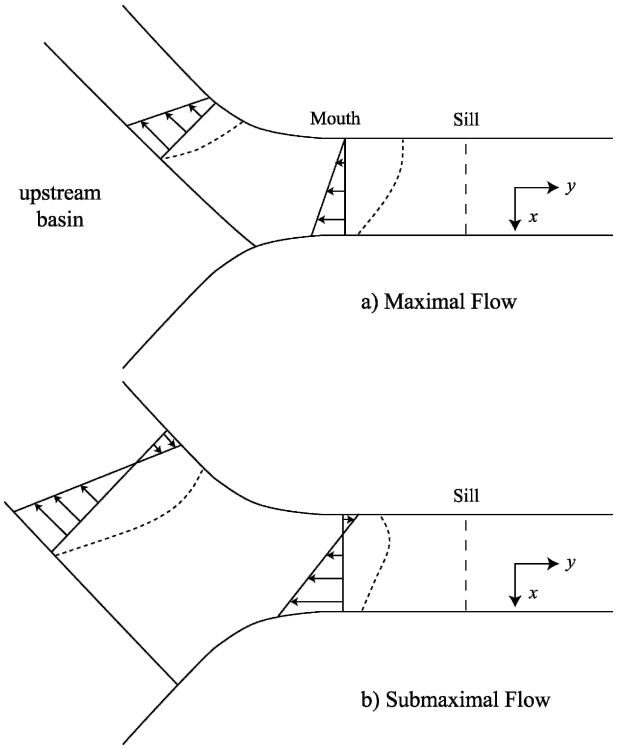

FIG. 10. Attached sill flow and surface flow in the mouth and upstream basin. The width of the surface boundary flow is w_e. The dotted lines indicate the position of the interface in the cross section.

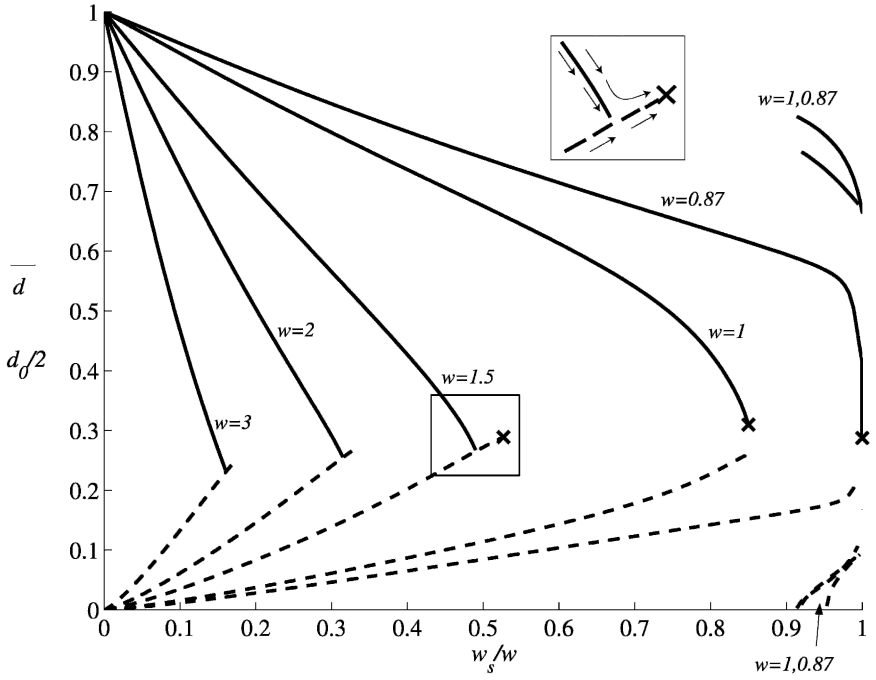

FIG. 11. Conditions at the mouth of the strait as a function of the relative width w_s/w of the singly detached flow at the sill. For solid curves the mouth flow is attached and has wall-averaged depth $\overline{d}$. For the dashed curves the mouth flow is detached and has left wall depth d_0. Crosses indicate the maximal state. A curve corresponding to a particular channel width w has upper and lower branches corresponding to subcritical and supercritical flows. When detachment occurs at the mouth the value of the subcritical root is the same as $d_0/2$ for the supercritical root, and the two curve branches therefore merge (see inset sketch). In the case $w = 0.87$, the sill flow becomes attached $w_s/w = 1$ before the mouth flows merge. For $w \geq 1.148$, the subcritical flow in the mouth detaches before merger with the (also detached) supercritical branch occurs. The widths w_e of the two roots remain distinct however. A further increase in w_s/w is needed to cause the solutions to merge and become critical (and maximal).

First, we seek physically meaningful attached flows in the mouth, linking to singly detached sill flows. Equation (39) is equated to (61), which yields

$$\overline{d}^3 + \overline{d}^2\left(\frac{\hat{v}_+\hat{v}_-}{2} + \frac{w_B^2}{8} - 1\right) + \frac{Q^2}{2w_B^2} = 0, \qquad (70)$$

where (60) has been used to eliminate $\hat{d}$. Solutions are shown by the solid curves in Fig. 11. The flow is detached at the mouth where the solid curves end.

If the mouth flow is detached, the upper layer continues into the upstream basin unaltered. Its width w_e is therefore the same as the width in the mouth. If the mouth flow is attached, the upper layer must move a finite distance into the basin before detachment occurs. In either case, the detached width w_e can be calculated by equating the Bernoulli functions (39) and (64) and using (65) and (66). The resulting relation

$$w_e^4 + 4w_e^2[\hat{v}_+\hat{v}_- + (2Q)^{1/2} - 2] + 8Q = 0, \qquad (71)$$

must be solved simultaneously with (41), (42), and (43). The results are displayed in Figs. 11 and 12. The former gives the wall depth d_0 (dashed curves) for detached flow in the mouth together with the previously discussed solid curves giving the average wall depth for attached mouth flows. For each w the composite of these curves has a subcritical (upper) branch and supercritical (lower) branch. There are some subtleties to the merger of the two curves, as explained in the figure caption.

A similar plot showing the subcritical and supercritical widths w_e in the basin appears in Fig. 12. Each curve corresponds to a particular w and is a composite of information calculated for attached, singly detached, and doubly detached sill flows (see next section) as coded by the different line styles. Merger of the subcritical and supercritical (upper and lower) branches of a curve for a particular w indicates critical, detached flow in the mouth and the upstream basin (both flows are detached) and therefore a maximal state. For

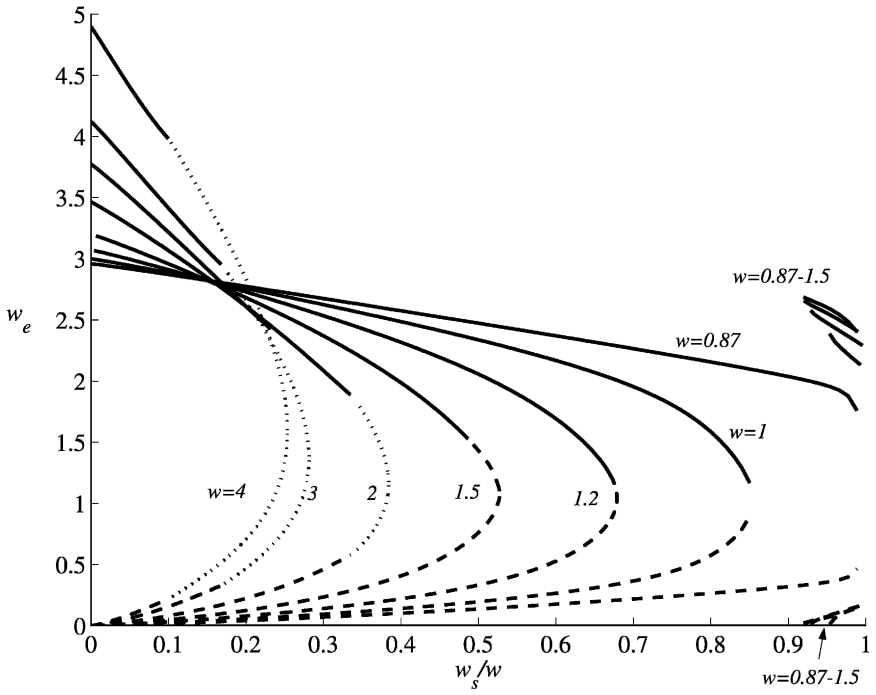

FIG. 12. Similar to Fig. 11, but now the detached width w_e of the flow in the upstream basin is plotted as a function of w_s/w. Dashed curves indicate that the mouth flow is detached; the upper-layer width there equals w_e. Solid curves indicate that the flow in the mouth is attached. Dotted curves indicate that the mouth flow is detached and that the sill flow is doubly detached; w_s should then be interpreted as $w + w_b - w_t$ as explained in Fig. 6. Maximal states occur when the mouth flow is critical and this may or may not correspond to merger of the subcritical and supercritical values of w_e. For $w \geq 1.148$, critical flow in the mouth is detached and therefore the critical state does correspond to such a merger. Maximal flow occurs when the subcritical and supercritical values of w_e merge. For $w < 1.148$, the critical mouth flow is attached and can be linked to distinct subcritical and supercritical values of the width w_e in the basin. The latter are the terminations of the dashed and solid curves corresponding, for example, to $w = 1$.

$w < 1.148$ the situation is complicated by the fact that critical flow in the mouth occurs under conditions of attachment. The corresponding upstream supercritical and subcritical values of w_e are distinct and are indicated by the terminations of the dashed and solid curves. This and other details are described in the caption.

The weir relation for singly and doubly detached sill flows is plotted in Fig. 13, which extends the (Q/w versus w_e) relation to higher values of w. The only solutions shown in Fig. 13 are ones for which the basin, mouth and sill flows can be dynamically connected. Note that this does not include the solutions given by the second set of curves around $w_s/w \approx 1$, shown in Figs. 4, 11, and 12, which cannot be dynamically connected.

d. Doubly detached sill flow

When the sill flow becomes doubly detached, which first occurs for $w = 1.544$ (for $w < 1.544$, the maximal state is attained before the flow detaches from both sidewalls), it can be shown that all consistent mouth flows are detached. The basin states are therefore identical to the states in the mouth. These upstream states can be found by equating (50) and (64), yielding the quartic equation of (71) in w_e, and this must be solved in conjunction with (52), (53), and (54). Various properties of the solution are plotted, including w_e versus w_s/w (Fig. 12), Q/w versus w_e (Fig. 13), and w_e/w versus w_t/w (Fig. 14). In each case, supercritical and subcritical branches of curves describing the upstream flow are possible and maximal flow occurs where these branches merge. For submaximal flow, the subcritical upstream state is appropriate. Under maximal conditions, the upstream flow is critical at the mouth and continues to be critical as the upper layer flows into the basin. Plan views showing each case appear in Fig. 15. It is questionable whether the uniform upstream critical flow predicted in the maximal case can actually be maintained.

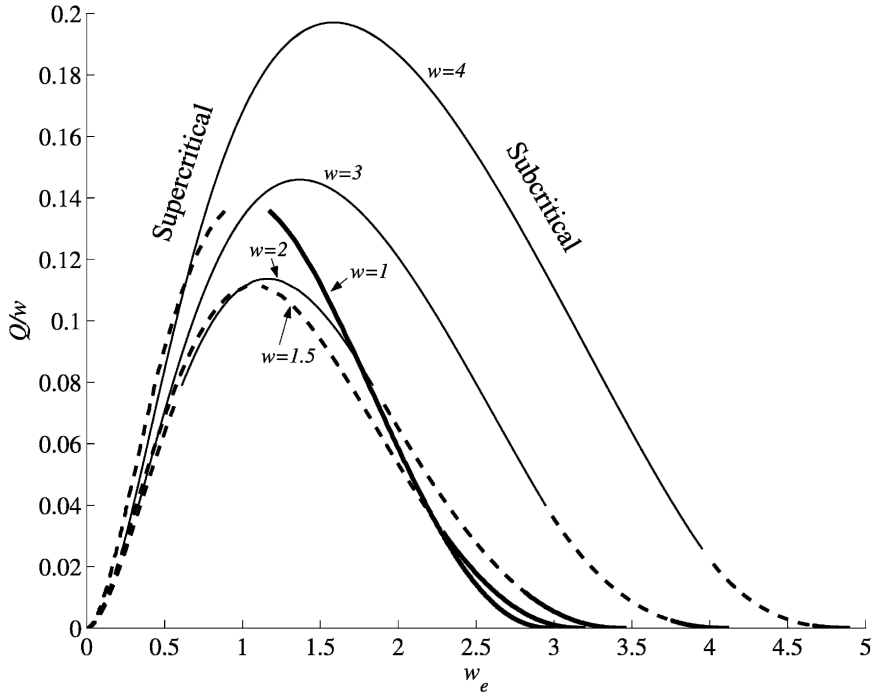

FIG. 13. Exchange flow rate as a function of the width w_e of the detached boundary current in the upstream basin. For the plots included, which are restricted to sill widths $w \geq 1$, the flow may be doubly detached at the sill and detached at the mouth (thin, solid curves), singly detached at the sill and detached at the mouth (dashed curves), or singly detached at the sill and attached at the mouth (thick, solid curves). Except for $w = 1$, the subcritical and supercritical (right and left) branches of each curve coalesce, indicating that the upstream boundary current is critical and the flow maximal. The mouth flow in each of these cases is detached and therefore identical to the basin flows. For $w = 1$ the mouth flow is attached and the upstream supercritical and subcritical values of w_e remain distinct.

An important finding, apparent in Fig. 13, is that the maximal flux increases with increasing w, reversing a trend established for attached and singly detached sill flows.

e. Summary of maximal states

Maximal exchange states are summarized in Fig. 16 and cross sections of the maximal exchange interface are shown in Fig. 17. The maximal exchange flux can be determined by the channel width and it is only necessary to know g', D_s, and f. That is, the sill flow is isolated from the up- and downstream basins on each side by a supercritical region so that it is independent of the properties in the upstream reservoir.

7. Application to the Strait of Gibraltar

The Strait of Gibraltar (Fig. 18) is about 60 km long and 20 km wide. It has a minimum width of about 13 km at the deep (about 800 m) Tarifa narrows and a shallow sill (<300 m) near Camarinal to the west. The main circulation in the strait is driven by an excess of evaporation in the Mediterranean Sea forming dense, salty water and the Atlantic is the source of low-density water in the exchange.

A key issue that remains an open debate is whether or not the exchange is maximal. If it is maximal, then conditions in the strait will respond relatively slowly to air–sea exchanges in the Mediterranean and exhibit small seasonal change. On the other hand, a submaximal exchange will exhibit relatively rapid responses (e.g., changes in interfacial depth) to mixing changes in the Mediterranean. Garrett et al. (1990a) indicate that the sea level gradient between the Atlantic and Mediterranean and interface depth in midstrait at the eastern end of the strait are different for maximal and submaximal states. They conclude based on sea level gradients along the strait and interfacial depth data across the eastern part of the strait that the exchange is generally maximal in the early part of the year and submaximal in the later part of the year.

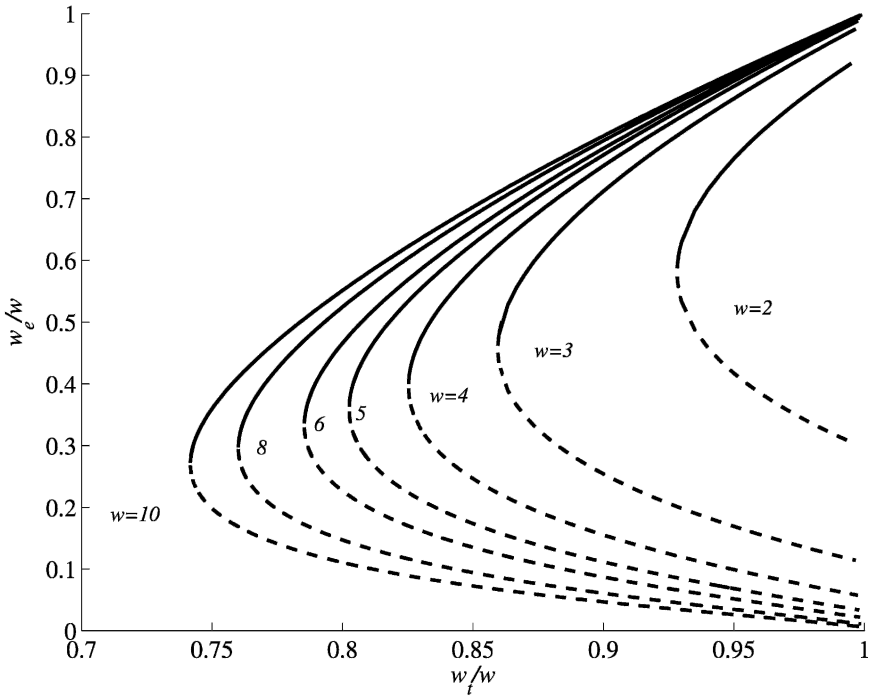

FIG. 14. The width w_e/w of the current in the upstream basin as a function of w_t/w at the sill crest for critical and doubly detached flow there. Critical flow occurs at the mouth, corresponding to maximal exchange, when subcritical solutions (solid curves) and supercritical solutions (dashed curves) coalesce.

Armi and Farmer (1988) describe the exchange in some detail. The dense water flows west and accelerates over Camarinal sill, which acts as a control. The fresher Atlantic water flows east into the western Mediterranean Sea (the Alboran Sea). It accelerates through Tarifa narrows, where there may be a second control point with supercritical flow to the east of this. If this is the case, the exchange is maximal, with supercritical flow just west of Camarinal sill, supercritical flow in the eastern narrow section of the Strait, and subcritical flow in between the two controls. By calculating two-layer Froude numbers (neglecting rotation) at various points along the strait, Farmer and Armi (1986) show that the flow through the strait is maximal except for a short portion of the tidal cycle. Bormans and Garrett (1989b) have found that a solution for the strait transport that is based on the average flow is essentially equivalent to the average solution of a model that includes tidal fluctuations so that a model that neglects tidal variability is adequate.

Acoustic images and CTD sections show the surface Atlantic layer entering the Alboran Sea with the interface intersecting the surface at some point between Tarifa and Gibraltar (see Armi and Farmer 1988, their Fig. 11). This phenomenon is associated with a frequently observed surface slick. Integration of the surface inflow yields estimates of 1 Sv (where 1 Sv $\equiv 10^6$ $m^3\,s^{-1}$) eastward transport (Armi and Farmer 1988). Below the inflow, the lower layer is deep and essentially inactive. Figure 19 shows an area of low reflectance south of Gibraltar, possibly indicating the separation of the Atlantic water from the European coast.

Typical cross sections of the Strait of Gibraltar are approximately parabolic. An effective depth at the sill is estimated to be $D_s = 200$ m by best approximating the parabolic shape as a rectangle. The local Rossby radius of deformation at the Camarinal sill section, based on this depth is $R = (g'D_s)^{1/2}/f \approx 23$ km, where $f = 8.5 \times 10^{-5}\ s^{-1}$ and $g' = 2 \times 10^{-2}\ m\,s^{-2}$ (Bormans and Garrett 1989a). The exchange flux as a function of the width of the upstream flow is shown in Fig. 20 for $w = 0.57$, the nondimensional width at Camarinal sill. The cross on the supercritical branch of the curve is the theoretical maximal exchange flux; this corresponds to a theoretical detachment width of $w_e = 0.66$ or a dimensional width of $w_e^* \approx 15$ km and an exchange flux $Q/w = 0.18$ or a dimensional exchange flux of $Q^* = Qg'D_s^2/f = 0.95$ Sv. The shaded portion of the curve gives the range for the expected exchange flux based on our estimate of the width of the Atlantic layer when it detaches from the European coast, $w_e^* = 15 \pm 1$ km, shown in Fig. 19. The width estimate is substantiated by

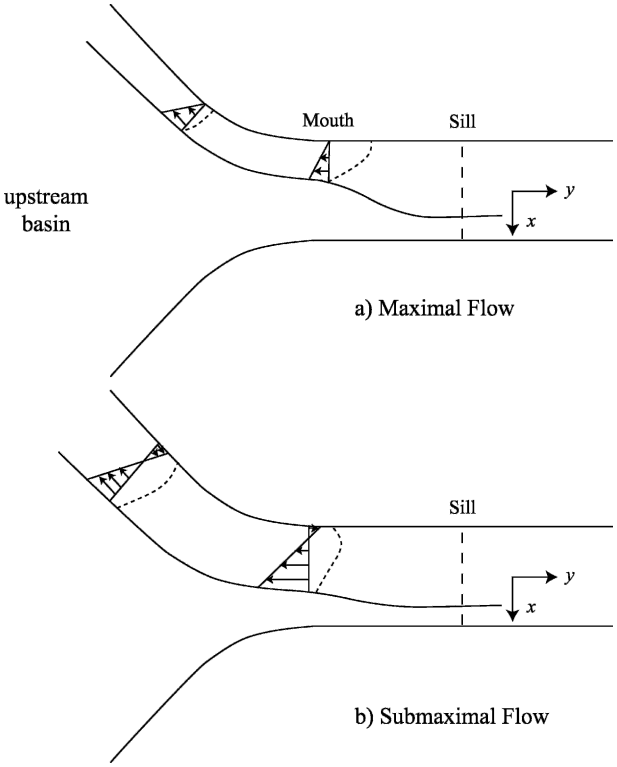

FIG. 15. Plan view of the doubly detached sill flow and surface flow in the mouth and upstream basin. The width of the surface boundary flow is w_e. The dotted lines indicate the position of the interface in the cross section.

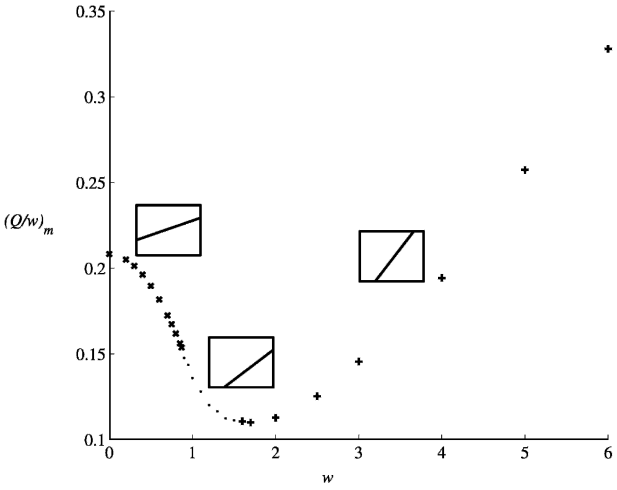

FIG. 16. Maximal exchange flux as a function of channel width for different critical sill states (attached, singly detached, and doubly detached).

Fig. 11 of Armi and Farmer (1988). This gives an exchange flux of $Q^* = 0.92 \pm 0.03$ Sv. Note that the w_e values corresponding to submaximal states (right-hand solid curve of Fig. 20) are considerably larger than observed.

The most recent published exchange estimates are given by Tsimplis and Bryden (2000) who average over a time series of Camarinal sill moored acoustic Doppler current profiler (ADCP) data between January and April 1997 to find a flux of -0.78 ± 0.17 Sv for the Atlantic inflow and 0.67 ± 0.04 Sv for the Mediterranean outflow. These values were found to be consistent with previous studies within the assumed errors. Hence, using our relationship between the width of the detached surface flow and the exchange flux, agreement is found with measured exchange fluxes, although at the upper limits of the expected values. Our predictions are made on the assumption of negligible net barotropic transport, while the effects of a net barotropic transport can include reverse and submaximal flows (Armi and Farmer 1986). Clearly, the predictions would also be influenced by the presence of a hydraulic jump between Tarifa narrows and the mouth at the Gibraltar–Ceuta section. However, there is no evidence of such a jump in any season (Bormans and Garrett 1989a). It may be possible that an abrupt change in topography may also force the upstream flow to separate, although it is unlikely in this case as separation appears to occur well before the Bay of Gibraltar.

Despite the uncertainties in our volume flux estimates, we can likely conclude that in October 1984 (the time of the shuttle photograph) the flow through the Strait of Gibraltar was maximal with supercritical flow in the upstream (Mediterranean) basin. This is in accordance with Armi and Farmer (1988) who give the impression that the exchange is maximal if the separation point is between Tarifa Narrows and Algeciras, although they do not prove this. Our theory maintains that submaximal exchange corresponding to a subcritical flow would clearly be evident since such a flow would have a separation width $w_e > 1.4$ or $w_e^* > 32$ km. A maximal flow state in October 1984 is further in accordance with the monthly mean sea level drop from the Atlantic to the Mediterranean (Garrett et al. 1990b and online at http://www.pol.ac.uk/psmsl/). The monthly mean sea level drop between Cadiz and Malaga in October 1984 is 0.19 m, close to the value (about 0.2 m) corresponding to a maximal state as discussed in Garrett et al. (1990b). Submaximal exchange has a mean sea level drop of only about 0.09 m (Garrett et al. 1990b). A time series of space images coinciding with sea level data would be very useful to determine over what timescale changes between submaximal and maximal flow occur, if at all, and whether the surface signature of such changes is indeed a change in the width of the upstream flow.

The surface Atlantic inflow curves southward and

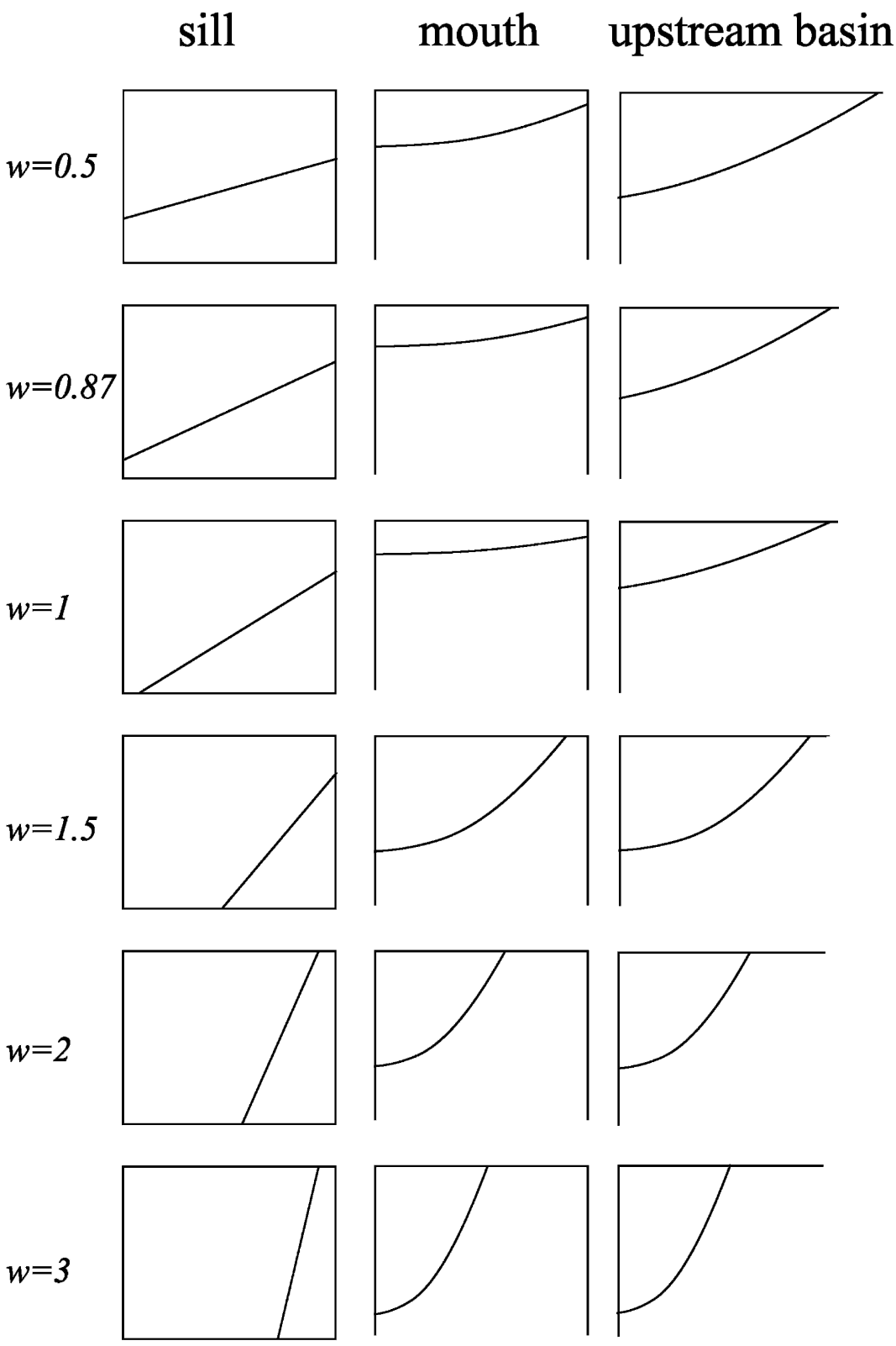

FIG. 17. Cross sections of maximal exchange configurations at the sill, mouth, and in the upstream basin.

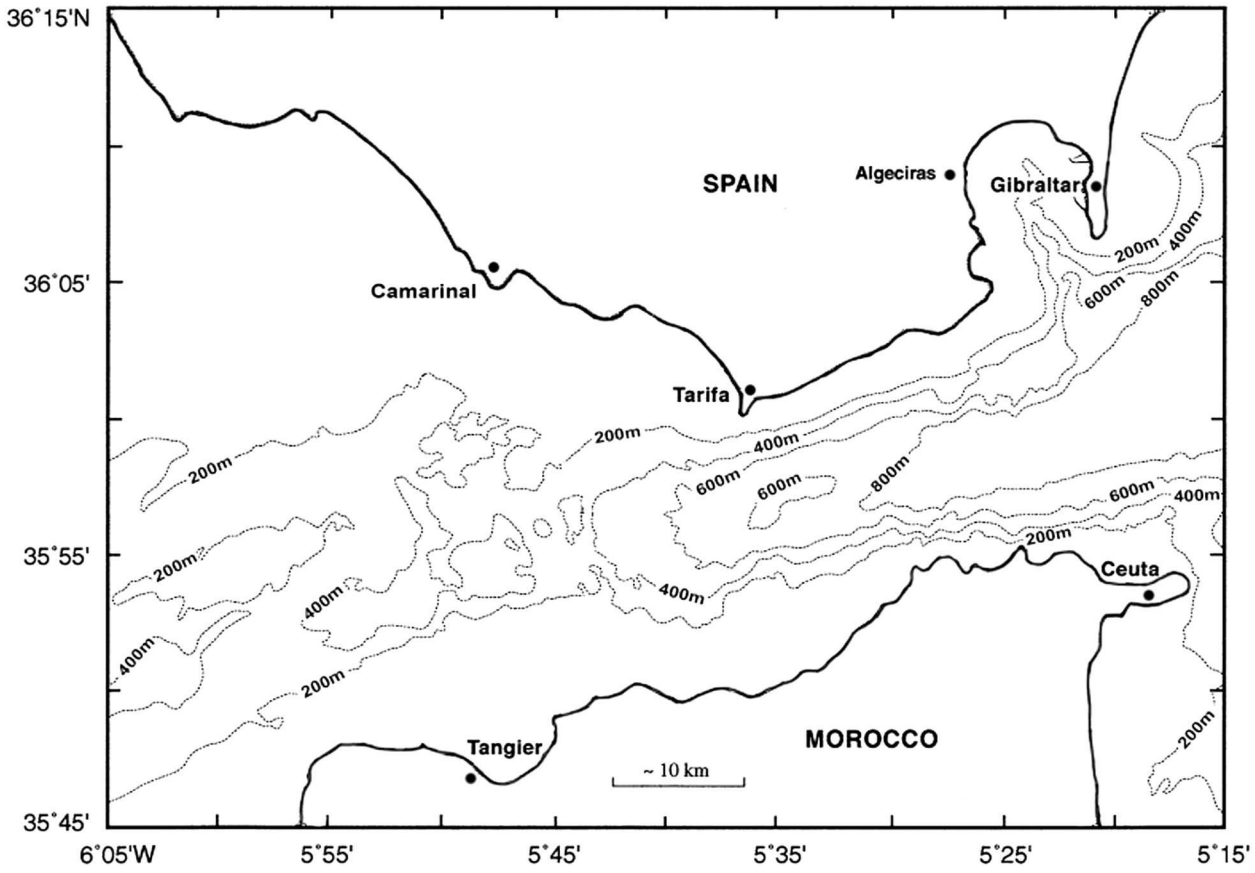

FIG. 18. Bathymetry of the Strait of Gibraltar showing the main sill at Camarinal and the narrows at Tarifa.

can form a large anticyclonic gyre in the Alboran Sea, while at other times it remains a coastal current that hugs the shore (see, e.g., Perkins et al. 1990). Based on the criterion of Bormans and Garrett (1989a), Garrett et al. (1990a) show that the presence of a gyre can be associated with both maximal and submaximal exchange through the Strait of Gibraltar, but that the exchange must be submaximal if the gyre is replaced by a coastal current. That is, the speed of a subcritical surface flow divided by the Coriolis parameter is insufficient for separation to occur (i.e., it is less than the radius of curvature of the boundary). Recall from section 6 that recirculations in upstream subcritical flows exist regardless of the geometry at the mouth. Hence, while not a gyre as such, a band of reverse (northwest) flow along the African coast may be expected in the submaximal case although it is unclear what role the geometry at the end of the channel would play.

8. Summary and conclusions

Critical conditions for distinct two-layer flow configurations at a sill in a rotating reference frame have been derived. Critical sill flow is always attached for $w \leq 0.866$, while it may be attached or singly detached for $w < 1.001$. For $w \geq 1.001$, it may be attached, singly detached or doubly detached. Submaximal to maximal

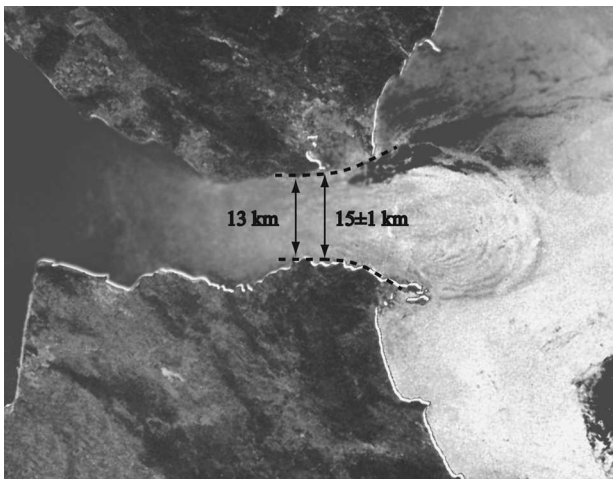

FIG. 19. Photograph of the Strait of Gibraltar taken in Oct 1984 from the space shuttle showing the area of low reflectance south of Gibraltar. NASA, LBJ Space Center Photo S-17–34–080.

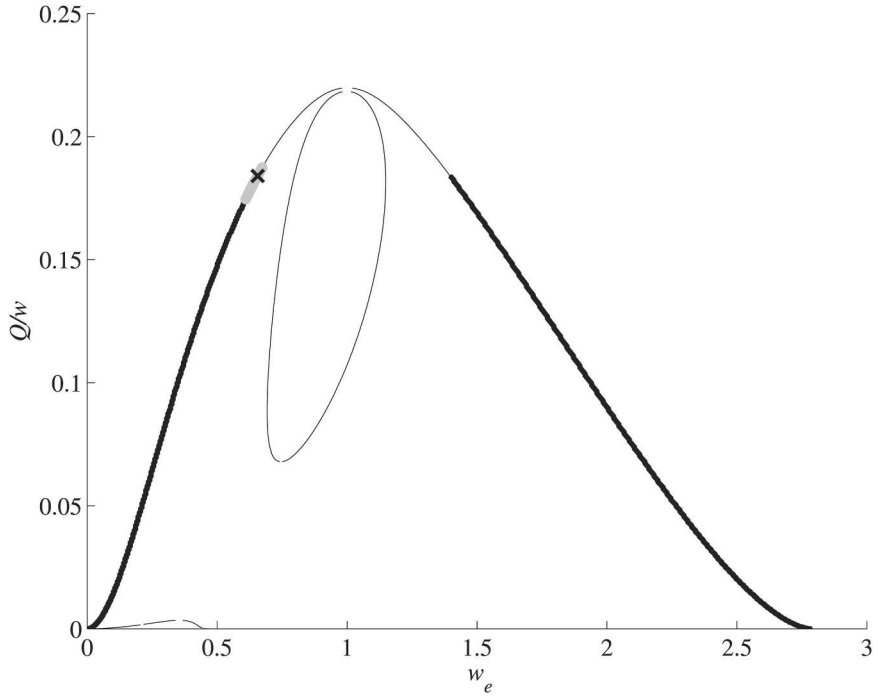

FIG. 20. Exchange flow rate as a function of the width w_e of the current in the upstream basin for critical and attached conditions at the Camarinal sill crest and $w = 0.57$. The realizable flows, shown by the thick curves, are those that can be dynamically connected from the sill to the mouth and basin with the same exchange flux and Bernoulli function. The cross indicates the theoretical maximal exchange flux and the shaded area indicates the range of states at Gibraltar based on an estimate of the separation width $w_e^* = 15 \pm 1$ km ($w_e = 0.65 \pm 0.04$) from the north coast.

exchange states over a variety of detachment scenarios have been found. The maximal state occurs when the sill flow is attached for $w \leq 0.881$, singly detached for $1.544 > w > 0.881$, and doubly detached for $w \geq 1.544$. The corresponding mouth flow is attached for $w < 1.148$ and detached for $w \geq 1.148$. Further, it has been shown that the exchange flux increases with increasing rotation for doubly detached sill flow. This is reasonable because of the larger velocities that must exist in wider channels, however, the stability of such solutions and the possible retarding effect of eddies is undetermined.

Upstream detachment of the upper layer always occurs in our model as a result of the fact that the basin is infinitely wide. The width w_e of the corresponding coastal current can be used as the basis for a "weir" relation. For submaximal flow, this relation is contained in Fig. 9 (for $w < 1$) or Fig. 13 (for $w \geq 1$). If the basin is not sufficiently wide to allow detachment, a weir relation can still be established in terms of a variable measured at the mouth. For example, the variable $\overline{d}$, measured at the mouth, can be related to $\overline{d}_{2c}$ using Fig. 8 and, in turn, to Q/w using Fig. 3. This procedure is valid when the sill flow is attached. For singly detached sill flow Figs. 11 and 4 can be used in the same manner. If the flow is maximal, one need only know the values of w^*, g', D_s, and f to obtain the transport (Fig. 16).

Detachment of the upper layer in the upstream basin also allows one to discriminate between submaximal and maximal conditions. Submaximal states are characterized by relatively large values of w_e and by recirculations along the left wall of the basin. Maximal states are characterized by smaller w_e values and unidirectional boundary current flow. Although these properties have been proven for a boundary current with zero potential vorticity, there is reason to believe that they are more general. Consider a flow with arbitrary potential vorticity but having zero alongshore velocity at the wall, as in Fig. 7b. If this current is uniformly displaced an infinitesimal distance onshore or offshore, a new flow with the same Q and same energy is created [Q is unaltered because the wall depth is unchanged; $B(\psi)$ is unaltered because the range of ψ is unchanged]. The infinitesimal displacement can therefore be thought of as a stationary wave of the original flow and its existence is tantamount to hydraulic criticality. In other

words, any geostrophic boundary current having zero wall velocity (and therefore a horizontal interface at the wall) is hydraulically critical. It is natural to suppose that wider states with the same potential vorticity distribution are subcritical and have reverse velocity along the wall, whereas narrower versions are supercritical and unidirectional.

The application of our theory to the Strait of Gibraltar demonstrates a new way of monitoring the transport and of distinguishing between submaximal and maximal exchange flows in a strait using photographs from space or satellite imagery. Our theory emphasizes the value of the upstream surface flow in characterizing the exchange state in straits even when rotation is not very important within the strait. This could be beneficial in suggesting locations and monitoring strategies for observational programs in straits.

APPENDIX

Regularity Conditions

a. Singly detached sill flow

The following is an example of the procedure used to determine the properties of a virtual control for a particular w. Consider the case where the sill flow is singly detached and the flow at the virtual control is either singly detached or attached. Begin by assuming singly detached flow at the virtual control. The corresponding regularity condition is given by (15) with $\gamma_1 = \hat{v}_-$, $\gamma_2 = \hat{v}_+$, and $\gamma_3 = w_s$, leading to

$$\begin{vmatrix} \partial G_1/\partial d & \partial G_1/\partial \hat{v}_+ & \partial G_1/\partial w_s \\ \partial G_2/\partial d & \partial G_2/\partial \hat{v}_+ & \partial G_2/\partial w_s \\ \partial G_3/\partial d & \partial G_3/\partial \hat{v}_+ & \partial G_3/\partial w_s \end{vmatrix} = 0, \tag{A1}$$

with the G functions defined by (40)–(42). Application of (A1) leads to

$$\begin{aligned} \frac{1}{2}\hat{v}_{-\upsilon} w_{s\upsilon}\{&2d_\upsilon w(\hat{v}_{-\upsilon} + \hat{v}_{+\upsilon} - w_{s\upsilon}) \\ &+ w\hat{v}_{-\upsilon}[\hat{v}^2_{+\upsilon} - \hat{v}^2_{-\upsilon} + w(\hat{v}_{+\upsilon} + \hat{v}_{-\upsilon})] \\ &- 2w_{s\upsilon}\hat{v}_{-\upsilon}[w_{s\upsilon}\hat{v}_{-\upsilon} + w^2 + 2w(\hat{v}_{+\upsilon} - w_{s\upsilon})]\} = 0, \end{aligned} \tag{A2}$$

where the subscript υ denotes the variable at the virtual control. The critical condition (43) for singly detached flow at the sill $d = 1$ is

$$\begin{aligned} \hat{v}_- w_s\{&w(3\hat{v}^2_+ - 6\hat{v}_+ w_s + 4w_s^2) - 6\hat{v}_- w(-\hat{v}_+ + 2w_s) \\ &+ \hat{v}^2_-[3w + 2w_s^2(-3\hat{v}_+ + 4w_s)]\} = 0, \end{aligned} \tag{A3}$$

and the critical condition for singly detached flow at the virtual control $d = d_\upsilon$ is given by

$$\begin{aligned} \hat{v}_{-\upsilon} w_{s\upsilon}\{&wd_\upsilon(3\hat{v}^2_{+\upsilon} - 6\hat{v}_{+\upsilon} w_{s\upsilon} + 4w^2_{s\upsilon}) \\ &- 6\hat{v}_{-\upsilon} wd_\upsilon(-\hat{v}_{+\upsilon} + 2w_{s\upsilon}) \\ &+ \hat{v}^2_{-\upsilon}[3wd_\upsilon + 2w^2_{s\upsilon}(-3\hat{v}_{+\upsilon} + 4w_{s\upsilon})]\} = 0. \end{aligned} \tag{A4}$$

The other equations come from equating volume fluxes at the sill and the virtual control

$$w_s^2\hat{v}_-\left(\frac{\hat{v}_+ + \hat{v}_-}{4} - \frac{w_s}{3}\right) = w^2_{s\upsilon}\hat{v}_{-\upsilon}\left(\frac{\hat{v}_{+\upsilon} + \hat{v}_{-\upsilon}}{4} - \frac{w_{s\upsilon}}{3}\right), \tag{A5}$$

equating energy fluxes between the two controls

$$\hat{v}_+\hat{v}_- - 2 = \hat{v}_{+\upsilon}\hat{v}_{-\upsilon} - 2d_\upsilon, \tag{A6}$$

and the conditions for no net flow at each of the two controls

$$w_s^2\hat{v}^2_- - w(\hat{v}_- - \hat{v}_+ - w + 2w_s) = 0, \tag{A7}$$

and

$$w^2_{s\upsilon}\hat{v}^2_{-\upsilon} - d_\upsilon w(\hat{v}_{-\upsilon} - \hat{v}_{+\upsilon} - w + 2w_{s\upsilon}) = 0. \tag{A8}$$

Equations (A2)–(A8) give us seven equations in seven unknowns: w_s, $\hat{v}_-$, $\hat{v}_+$ at the sill and $w_{s\upsilon}$, $\hat{v}_{-\upsilon}$, $\hat{v}_{+\upsilon}$, d_υ at the virtual control.

If the flow at the virtual control is attached the regularity condition is given by (33). Equating volume fluxes between the sill and the virtual control [see (29) and (41)] yields

$$\begin{aligned} &\left[\frac{w_s^2}{w}\hat{v}_-\left(\frac{\hat{v}_+ + \hat{v}_-}{4} - \frac{w_s}{3}\right)\right]^2 \\ &= \frac{[\overline{d}_{2\upsilon}(d_\upsilon - \overline{d}_{2\upsilon}) - w^2 d_\upsilon/12]^3}{d_\upsilon[\overline{d}_{2\upsilon}(d_\upsilon - \overline{d}_{2\upsilon}) - w^2 d_\upsilon/12 + (d_\upsilon - 2\overline{d}_{2\upsilon})^2]}. \end{aligned} \tag{A9}$$

Equating energies between the sill and the virtual control [see (26) and (40)] yields

$$\begin{aligned} \hat{v}_+\hat{v}_- - 2 = &\frac{[\overline{d}_{2\upsilon}(d_\upsilon - \overline{d}_{2\upsilon}) - w^2 d_\upsilon/12](d_\upsilon - 2\overline{d}_{2\upsilon})}{[\overline{d}_{2\upsilon}(d_\upsilon - \overline{d}_{2\upsilon}) - w^2 d_\upsilon/12 + (d_\upsilon - 2\overline{d}_{2\upsilon})^2]} \\ &- 2d_\upsilon + 2\overline{d}_{2\upsilon}. \end{aligned} \tag{A10}$$

We again use the conditions (A3) and (A7). Hence there are five equations in five unknowns: w_s, $\hat{v}_-$, $\hat{v}_+$ describing the singly detached flow at the sill and d_υ, $\overline{d}_{2\upsilon}$ describing the attached flow at the virtual control. There are no valid solutions to these equations and we conclude that the virtual control sections (other than at the mouth) corresponding to singly detached sill flow have singly detached flow.

b. Doubly detached sill flow

The regularity condition for doubly detached flow at a virtual control is obtained by applying (15) to the system (51)–(53) with $(\gamma_1, \gamma_2, \gamma_3) = (\hat{v}_-, \hat{v}_+, w_t)$ as

$$\begin{vmatrix} \partial G_1/\partial d & \partial G_1/\partial \hat{v}_+ & \partial G_1/\partial w_t \\ \partial G_2/\partial d & \partial G_2/\partial \hat{v}_+ & \partial G_2/\partial w_t \\ \partial G_3/\partial d & \partial G_3/\partial \hat{v}_+ & \partial G_3/\partial w_t \end{vmatrix} = 0. \quad \text{(A11)}$$

The resulting condition yields

$$\begin{aligned} 2\hat{v}_{-\upsilon}^2\{&\hat{v}_{-\upsilon}^2 d_\upsilon[(w_{t\upsilon} + w) + (\hat{v}_{+\upsilon} - \hat{v}_{-\upsilon})/2] \\ &+ w w_{t\upsilon} \hat{v}_{-\upsilon}(\hat{v}_{-\upsilon}(w_{t\upsilon} + \hat{v}_{+\upsilon}) - 2d_\upsilon) \\ &+ d_\upsilon w(d_\upsilon - \hat{v}_{-\upsilon}\hat{v}_{+\upsilon}) \\ &- w_{t\upsilon}\hat{v}_{-\upsilon}^3(w + w_{t\upsilon} + \hat{v}_{+\upsilon} - \hat{v}_{-\upsilon})\} = 0. \quad \text{(A12)} \end{aligned}$$

The procedure for finding the virtual control for a given w depends on whether the sill flow is attached, singly detached, or doubly detached and is similar to the procedure described in section a of this appendix. However, no such virtual controls were found.

REFERENCES

Armi, L., 1986: The hydraulics of two flowing layers with different densities. *J. Fluid Mech.,* **163,** 27–58.

——, and D. M. Farmer, 1986: Maximal two-layer exchange through a contraction with barotropic net flow. *J. Fluid Mech.,* **164,** 27–51.

——, and ——, 1988: The flow of Mediterranean water through the Strait of Gibraltar. *Progress in Oceanography,* Vol. 21, Pergamon, 1–105.

Bormans, M., and C. Garrett, 1989a: A simple criterion for gyre formation by the surface outflow from a strait, with application to the Alboran Sea. *J. Geophys. Res.,* **94** (C9), 12 634–12 644.

——, and ——, 1989b: The effects of nonrectangular cross section, friction, and barotropic fluctuations on the exchange through the Strait of Gibraltar. *J. Phys. Oceanogr.,* **19,** 1543–1557.

Dalziel, S., 1988: Two-layer hydraulics: Maximal exchange flows. Ph.D. thesis, Department of Applied Mathematics and Theoretical Physics, University of Cambridge, 201 pp.

——, 1990: Rotating two-layer sill flows. *The Physical Oceanography of Sea Straits*, L. Pratt, Ed., Kluwer Academic, 343–371.

Farmer, D. M., and L. Armi, 1986: Maximal two-layer exchange over a sill and through the combination of a sill and contraction with barotropic flow. *J. Fluid Mech.,* **164,** 53–76.

Garrett, C., M. Bormans, and K. Thompson, 1990a: Is the exchange through the Strait of Gibraltar maximal or submaximal? *The Physical Oceanography of Sea Straits*, L. Pratt, Ed., Kluwer, 271–294.

——, K. Thompson, and W. Blanchard, 1990b: Sea-level flips. *Nature,* **348,** 292.

Gill, A. E., 1977: The hydraulics of rotating-channel flow. *J. Fluid Mech.,* **80,** 641–671.

Hogg, N. G., 1983: Hydraulic control and flow separation in a multi-layered fluid with applications to the Vema Channel. *J. Phys. Oceanogr.,* **13,** 695–708.

——, 1985: Multilayer hydraulic control with application to the Alboran Sea circulation. *J. Phys. Oceanogr.,* **15,** 454–466.

Hunkins, K., and J. A. Whitehead, 1992: Laboratory simulation of exchange through Fram Strait. *J. Geophys. Res.,* **97,** 11 299–11 321.

Perkins, H., T. Kinder, and P. La Violette, 1990: The Atlantic inflow in the western Alboran Sea. *J. Phys. Oceanogr.,* **20,** 242–263.

Pratt, L. J., and K. Helfrich, 2005: Generalized conditions for hydraulic criticality of oceanic overflows. *J. Fluid Mech.,* in press.

——, H. E. Deese, S. P. Murray, and W. E. Johns, 2000: Continuous dynamical modes in straits having arbitrary cross sections, with applications to the Bab al Mandab. *J. Phys. Oceanogr.,* **30,** 2515–2534.

Riemenschneider, U., 2004: The dynamics of two-layer rotating exchange flows—An analytical and numerical modeling study. Ph.D. Thesis, University of Southampton, 187 pp.

Smeed, D., 2000: Hydraulic control in three-layer exchange flows and application to the Bab al Mandab. *J. Phys. Oceanogr.,* **30,** 2574–2588.

Stern, M. E., 1980: Geostrophic fronts, bores, breaking and blocking waves. *J. Fluid Mech.,* **99,** 687–703.

Tsimplis, M. N., and H. L. Bryden, 2000: Estimation of the transports through the Straight of Gibraltar. *Deep-Sea Res.,* **47A,** 2219–2242.

Whitehead, J. A., A. Leetmaa, and R. A. Knox, 1974: Rotating hydraulics of strait and sill flows. *Geophys. Fluid Dyn.,* **6,** 101–125.

Wood, I. R., 1968: Selective withdrawal from a stably stratified fluid. *J. Fluid Mech.,* **32,** 209–223.